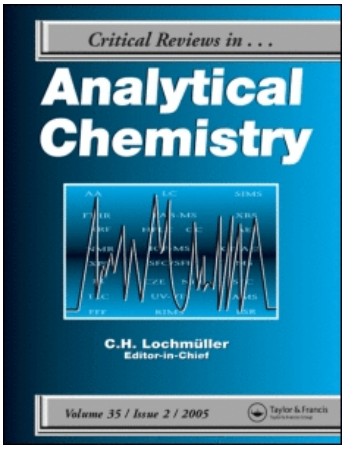


**Critical Reviews in Analytical Chemistry**
Publication details, including instructions for authors and subscription information:
http://www.informaworld.com/smpp/title~content=t713400837

# Particle Size Measurement Using Chromatography

Anthony J. McHugh; Howard Brenner

**To cite this Article** McHugh, Anthony J. and Brenner, Howard(1984) 'Particle Size Measurement Using Chromatography', Critical Reviews in Analytical Chemistry, 15: 1, 63 — 117
**To link to this Article: DOI:** 10.1080/10408348408542776
**URL:** http://dx.doi.org/10.1080/10408348408542776

# PARTICLE SIZE MEASUREMENT USING CHROMATOGRAPHY

Author: **Anthony J. McHugh**
Department of Chemical Engineering
University of Illinois
Urbana, Illinois

Referee: Howard Brenner
Department of Chemical Engineering
Massachusetts Institute of Technology
Cambridge, Massachusetts

## TABLE OF CONTENTS

# I. INTRODUCTION

## A. Background and Overview

Determination of the particle size (PS) and particle size distribution (PSD) is one of the most important aspects of the characterization of particulate systems, whether in a powdered, latex, or suspension form. The importance of particle size analysis to the various fields of particle science and technology rests on the wide range of properties which are directly relatable to the PS and PSD. These vary from fundamentally important phenomena such as the stability, light scattering, and viscosity behavior of particulate suspensions, to practically important properties such as the covering power, gloss, and surface protection characteristics of coatings and paints. The number of techniques available is enormous[1,2] and the particular method best suited to a given application will depend primarily on the size or size range in question and whether one is interested in determining an average size or the complete size distribution. A relatively recent review paper[3] gives a good overview of the most commonly used and pertinent techniques along with a discussion of the relative merits of the key methods.

In this review, discussion will be focused on a relatively recent development in the analysis of colloidal size particles, namely the application of liquid chromatography techniques to the size determination. The most predominant use of these techniques has been with polymer colloidal latex systems in which the polymeric particles are charged (by ionogenic surface groups and/or adsorbed ionic stabilizing species) and generally spherical in shape ranging from a few hundred Angstrom units in diameter to several microns. Growth of this field of analysis has been dramatic and several distinct methods have emerged, each with names suggestive of different separation mechanisms. The three major areas of particle chromatography can be classified into packed column systems, open capillary tubular systems, and so-called field flow fractionation systems.



## B. Methods of Particle Chromatography

A classification of the various particle chromatography methods is illustrated in Figure 1. The packed column methods stem from experimental studies[4,5] which demonstrated that suitably stabilized, dilute suspensions of latex particles will fractionate according to size when pumped through beds of porous or nonporous beads. In the case of the nonporous systems, separation occurs primarily as a result of the finite size of the solute particles and their preferred sampling of the faster moving eluant streamlines in the interstices of the packing. As a consequence, the term "hydrodynamic chromatography" (HDC) has been used to describe the process.[5,10] Under conditions where van der Waals attractive forces between the particle and packing surfaces are predominant, the possibility exists for a controlled deposition-reintrainment process to occur. Such behavior would depend on the physicochemical parameters which control the potential energy of interaction between the particle and packing surfaces, as well as the particle size. For such cases the term "potential barrier chromatography" (PBC) has been used to describe the process.[15,16]

In the case of porous packed systems, a clear delineation of the separation mechanisms is more difficult. Some experimental studies have indicated that a two-phase, partitioning process is possible when packing pore diameters are in the ranges generally associated with classical liquid or size exclusion macromolecular chromatography,[17,18] hence the system can be described as liquid exclusion. However, as the pore size increases, the possibility exists for purely flow-through channels to exist in the bed, in which case the term "porous hydrodynamic chromatography" has been used since it is more suggestive of the controlling mechanism.[9]

The open tube capillary method referred to as "capillary hydrodynamic chromatography" has been applied to the analysis of submicron-sized particles and particles above a micron

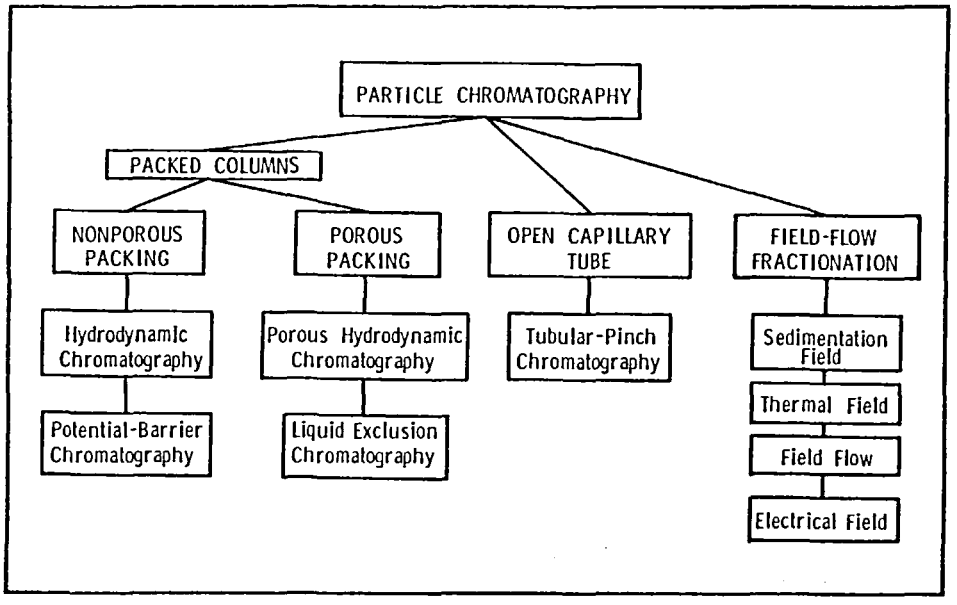


FIGURE 1. Classification of principal areas of particle chromatography. (From McHugh, A. J., Nagy, D. J., and Silebi, C. A., Size Exclusion Chromatography (GPC), *ACS Symp. Ser. 138*, Proudet, T., Ed., American Chemical Society, Washington, D.C., 1980, 1. With permission.)

in diameter as well.[19,20] It is not clear at this point whether a precise carryover of the HDC mechanism can be used to explain the separation in the submicron range. On the other hand, the mechanism for the larger particles appears to be due to the "tubular pinch effect". In this case, studies have shown that under certain flow conditions an initially homogeneous suspension of neutrally buoyant particles flowing through a constant diameter tube of circular cross section will tend to concentrate or "pinch" into an annular ring near the tube center. The precise annular position depends on the particle size, and since velocity varies radially, a separation of different-sized particles can be induced by this mechanism. For this reason, the process has been labeled as "tubular pinch chromatography".

Another area of rapid growth for particle sizing has been that of field-flow fractionation (FFF), developed largely by Giddings.[21-23] Like HDC, field-flow fractionation is achieved by means of external forces rather than a partitioning between two phases, and is thus a one-phase chromatographic system. In FFF, as a carrier stream moves through a flow channel, an external force field or gradient is applied at right angles to it. The field interacts with the solute forcing it to form a thin layer against the wall which is then sorted according to size by the flow field. A variety of separations have been successfully performed on viruses, proteins, linear polystyrenes, latex particles, silica beads, and pigments using various forms of FFF.

The objective in this review will be to present an overview and discussion of these various methods of particle chromatography. Since development of the techniques of packed column chromatography has occurred rapidly in the last 6 years and, as yet, no comprehensive review of the subject has been published, this area will be emphasized. It is hoped that a critical review comparing the techniques, data analysis, and separation mechanisms of these two methods will be both timely and instructive. The discussions of capillary HDC and field-flow fractionation will be somewhat less comprehensive, in the former case because of the limited literature on the subject and, in the latter case, because extensive treatments can be found elsewhere.[21-23] On the other hand, some overview of these techniques is clearly warranted on the basis that insights into their range of usefulness as well as an appreciation

**Table 1**
**MACROMOLECULAR SEC AND PARTICLE CHROMATOGRAPHY SYSTEMS**

TYPICAL OPERATION FEATURES

| | SEC[6] | Particle chromatography |
|---|---|---|
| Columns | | |
| Type | Stainless steel | Stainless steel or glass |
| I.D. | ~1/2 cm | ~1/2—1 cm |
| Length/column | ~50 cm | ~50—150 cm |
| Packing | | |
| Type | Organic gels/silica particles | Sty-DVB particles/glass spheres/LEC porous glass |
| Size | 5—30 μm | 18—60 μm |
| Porosity | 6—400 nm | Nonporous or if porous, generally 500 nm to several μm |
| Detectors | Refractive index, low angle laser scattering | Turbidity, refractive index |
| Solute size range | ~$10^3$—$10^7$: M.W. | ~30—500 nm: $D_p$ |

of the similarities and differences as regards separation mechanisms and methods of analysis can thereby be gained.

## II. PACKED COLUMN PARTICLE CHROMATOGRAPHY

One can point to several probable reasons to explain the rapid development of the packed column methods. Before entering into a detailed description of these techniques, it is worthwhile to consider some general comments regarding this.

In the first instance, although the packed column methods can be used to analyze a fairly wide range of particle sizes (depending on the packing diameter used), the most efficient operation occurs in a size range which has traditionally been difficult to analyze, this being particle diameters ranging from several hundred Angstroms to less than 0.5 μm in diameter. Techniques such as electron microscopy, light scattering, centrifugation, electrozone sensing (e.g., Coulter counter), fractional creaming, and small angle scattering have generally been used in this range.[3] However, these methods are often time consuming and generally unsuitable as quality control methods. In addition, their accuracy is often limited to fairly narrow-size distribution systems. Consequently, due to their speed and accuracy, packed column chromatographic methods are rapidly becoming preferred techniques. It seems clear now that the development of these techniques to a high performance status will have much the same impact on the science and technology of submicron colloidal systems as size exclusion chromatography has had on the field of macromolecular analysis.

Secondly, due to the strong similarities between HDC and the more fully developed methods of macromolecular size exclusion chromatography (SEC), a direct carryover of techniques and methods of analysis has been possible. By way of example, a general comparison of the typical operating features of the two methods is illustrated in Table 1. In both cases one is dealing with systems consisting of small bore columns, packed with porous or nonporous beads. The packing porosity and pore size range plays an important role in controlling the separation mechanism and resolution of an SEC system,[6] while for porous particle chromatography applications it is not yet clear what the precise delineation of the separation mechanisms and resolution capacity is. The solute size ranges are molecular weights for SEC and spherical particle diameters for particle chromatography.

When one considers that the transport properties of a random macromolecular coil are often rationalized by treating it as a roughly spherical particle having a diameter on the order of twice the coil radius of gyration[7] (~100 to ~1000 Å), it would not seem unreasonable to expect that a strong correlation should also exist between the fractionation mechanisms as well as the operating characteristics of the two systems. Also, as will be shown in this review, many of the powerful methods developed for band broadening correction in size exclusion chromatography[8] can be carried over, with modification, to the development of algorithms for obtaining a complete particle size distribution from the output chromatogram.

Thus, on a superficial basis, it would seem that particle chromatography and macromolecular SEC are simple variations describable by much the same formalism. On closer inspection, however, important distinctions arise and an appreciation of these features is critical. To begin with, it seems well established that fractionation in SEC occurs as a consequence of an entropic, conformationally driven partitioning of the flexible macromolecular coils between the stationary porous phase and mobile solvent phase, with little or no so-called hydrodynamic separation effects occurring in the mobile phase.[6] Mathematical models for SEC, coupling the transport properties of flexible coils with the partitioning behavior, have been successful in describing many of the important features of the separation dynamics. When one considers the transport behavior of submicron colloidal systems, however, size-dependent hydrodynamic factors, as well as electrochemical force field effects enter into the convected Brownian motion and phase partitioning behavior. These lead to phenomena not generally observed with macromolecular systems. Fortunately, a fundamental basis for analyzing these effects is available and, as a consequence, a good deal of progress has been made in modeling many of the important details of particle chromatography separation mechanisms. This is an important consideration, since the utility of any analytical technique rests largely on the ability to describe accurately the effects one is attempting to control and use.



## A. Hydrodynamic Chromatography (HDC)

As indicated, the technique of column particle chromatography which employs nonporous packing has come to be known as hydrodynamic chromatography. The method was developed for polymer latex particles in the pioneering study by Small,[5] however, Pedersen[11] was probably the first to report that a separation of protein molecules could be obtained by passing them through a column packed with glass spheres of suitably small diameter. It is in some ways ironic that the separation mechanism which, with suitable modification, describes particle HDC, was originally proposed as a mechanism to explain macromolecular gel permeation chromatography,[12-14] a view which has since been superseded by the size exclusion approach.[6] In this section, the principal operating characteristics of HDC will be described, followed by a discussion of the separation mechanisms.

### *1. HDC Experiment*

Figure 2 shows a schematic illustration of a typical HDC apparatus. In appearance it is very similar to standard liquid chromatographic systems.[6] The instrument consists of a solvent delivery pump, pulse dampener, sample injection valve, one or more packed columns, a detection device, and strip chart recorder. Applications to polymer latex systems typically involve distilled water as the eluant phase, with suitable stabilizing agents dissolved in it such as ionic surfactants or low molecular weight salts.[5,9,10,24-26] Latex samples are normally injected into the columns at concentrations of 0.005 to 0.1% by weight along with trace amounts of a suitable marker species, typically 0.02% sodium dichromate. In Small's studies,[5,10] and most of those following,[9,24-26,28] 3 glass columns — 110 cm in length and 9 mm i.d. — were used, although stainless-steel columns are perhaps more attractive for high flow-high performance operation.[27] A range of packing materials was studied by Small,[5]

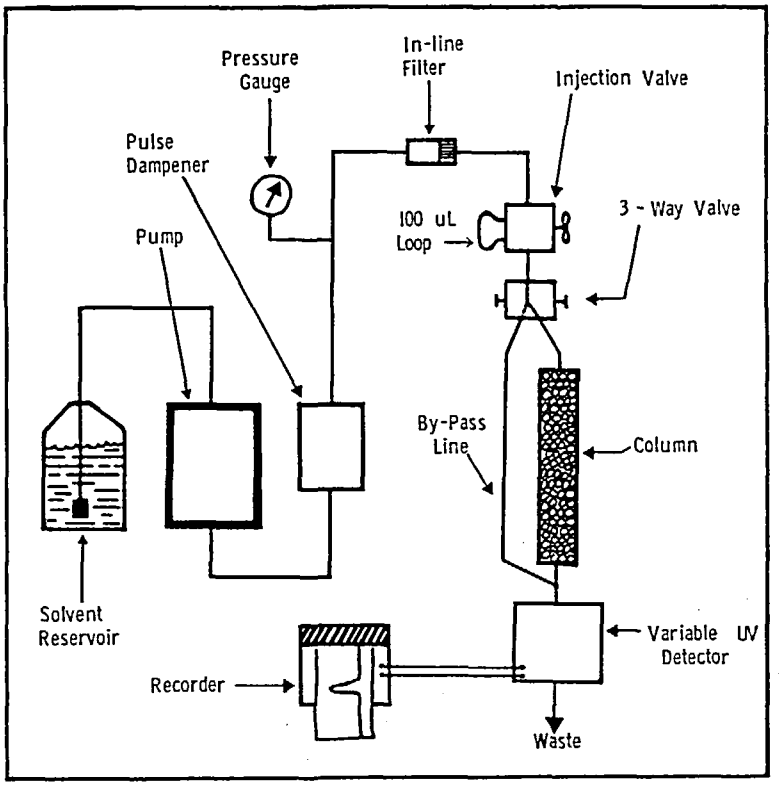


FIGURE 2. Schematic diagram of a typical HDC apparatus.

however, the principal features are that they be monodisperse (or nearly so) in size, nonporous, and inert. Styrene-divinylbenzene copolymer beads or cation exchange resins appear to be the most attractive. Detection and measurement of the colloid and marker species in the effluent are determined by monitoring turbidity either at a fixed wavelength of 254 nm[5], or, as to be discussed, using a variable wavelength UV system. Eluant normally circulates continuously through the column and the stabilized particles along with marker are injected into the head of the column train. Elution times for latex samples through a three-column system are typically 2 hr at a flow rate of 0.5 mℓ/min, however, with recent improvements this has been reduced to times on the order of minutes.[27]

A fairly extensive range of latex systems has been employed in HDC. Table 2 shows a summary of the published systems. However in terms of operational characteristics studies and studies of column separation mechanisms, the Dow monodisperse, polystyrene latexes have been the particles of choice since they are available in a convenient range of sizes and are well characterized.

Under typical operating conditions, larger latex particles elute from the columns ahead of smaller ones, including the marker species. Figure 3[29] shows an example of a chromatogram output of a mixture of 234- and 91-nm diameter particles.

The relevant experimental parameters involved in the HDC separation process are the latex particle size, ionic strength of the eluant, surfactant species and concentration, packing diameter, and eluant flow rate.

### 2. *Characteristics of the HDC Separation Factor, $R_F$*

The rate of transport of colloidal particles through the packed bed is conveniently expressed in terms of the separation factor, $R_F$, which is defined as the ratio of elution volumes associated with the marker peak, $V_m$, and the particle peak, $V_p$:

## Table 2
## SUMMARY OF HDC OPERATING CONDITIONS[5,10,26,34]

| Latex type | Size range (nm) | Eluant-added species | Packing types and sizes |
|---|---|---|---|
| | | **Surfactants** | |
| Polystyrene | 33—357 monodisperse | Sodium dihexylsulfosuccinate (AMA) | Styrene-divinylbenzene copolymer beads (20 μm) |
| Poly(vinyl chloride) | 37—145 monodisperse<br>116—214 polydisperse | Sodium lauryl sulfate (SLS)<br>Triton X-100 | |
| | | **Ionic species** | |
| Butadiene-styrene copolymer | 89 monodisperse | Disodium hydrogen phosphate<br>Sodium chloride | Sulfonated styrenedivinyl benzene copolymer resins (18, 40, and 58 μm)<br>Dowex 50x-8 exchange resin (68—120 μm)<br>Glass spheres |
| Carboxylated 70:30 styrene-butadiene copolymer | 70—230 monodisperse | | |
| Carboxylated 55:45 styrene-butadiene copolymer | 122—173 polydisperse | | |
| Polybutadiene | 132—290 polydisperse | | |
| Acrylate ester copolymer | 417 polydisperse | | |
| Poly(methyl methylacrylate) | 219—415 monodisperse | | |
| Poly(bromo styrene) | 196—302 monodisperse | | |
| Styrene-butadiene-acrylic acid copolymer (various compositions) | Sizes not reported | | |
| Styrene-butadiene-vinyl acid copolymer (various vinyl acids) | Sizes not reported | | |



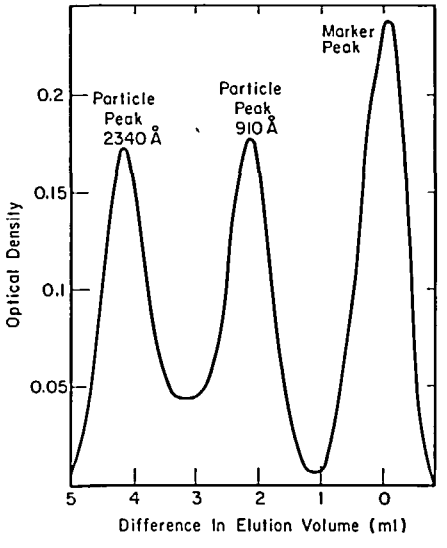


FIGURE 3. Chromatogram of polystyrene latex sample containing particles with diameters of 234 and 91 nm. (From Stoisits, R. F., Analysis of Colloids by Hydrodynamic Chromatography, M.S. thesis, Lehigh University, Bethlehem, 1975. With permission.)

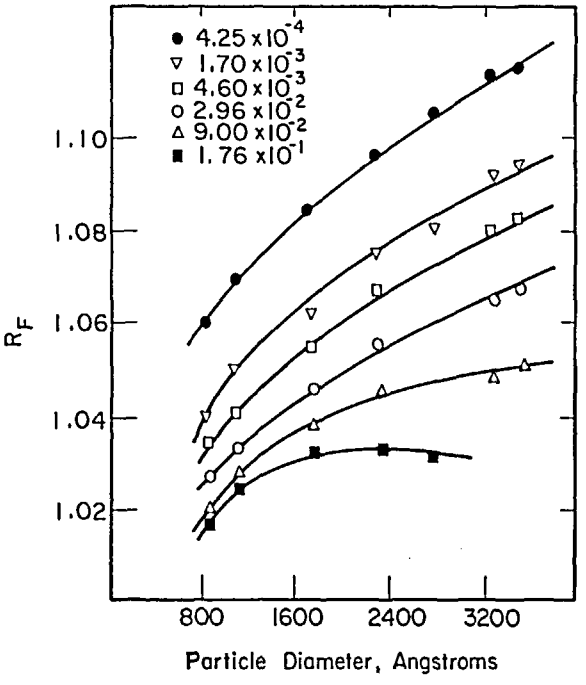


FIGURE 4. Separation factor-particle diameter data for various eluant ionic strengths. (From Small, H., *J. Colloid Interface Sci.*, 57, 337, 1976. With permission.)

$$R_F = \frac{V_m}{V_p} \tag{1}$$

An acceptable marker species should pass through the bed interstices with the same average velocity as the carrier or eluant phase. The dichromate ion, $Cr_2O_7^=$, which is detected due to its strong absorbance at 254 nm, is a suitable marker; however, it does show a slight dependence of elution time on the eluant ionic strength. This has been attributed to exclusion of the marker from the ionic double layer surrounding the packing.[5] These differences in elution times are less than 3% and do not affect the main conclusions drawn from the values of $R_F$, however, they are accounted for in the model calculations to be discussed later. Thus, in general, the elution volume, $V_m$, will be less than the total column void volume, $V_c$.

Figure 4 shows data taken from Small's study[5] illustrating the dependence of $R_F$ on particle diameter for various total ionic strengths of the species in the eluant phase. One sees that over a range of ionic strengths $R_F$ increases with increasing particle size which, straightaway, serves as the basis for the size separation. In addition, $R_F$ is always greater than unity, which means that the average velocity of the latex particles exceeds that of the eluant marker species. This is in sharp contrast to classical chromatography, where for a variety of reasons solutes are usually retarded in their movement through the column in which case $R_F \leq 1$.[31] One also notes that at higher ionic strengths $R_F$ decreases and eventually the separation behavior reverses, with smaller particles eluting ahead of larger ones. Similar behavior occurs with ion exchange resin and glass packings.

An alternate approach is to express the separation in terms of the elution volume difference between the particle and marker peaks, $\Delta V$. The separation factor and $\Delta V$ are related by:

$$\Delta V = V_m(1 - 1/R_F) \tag{2}$$

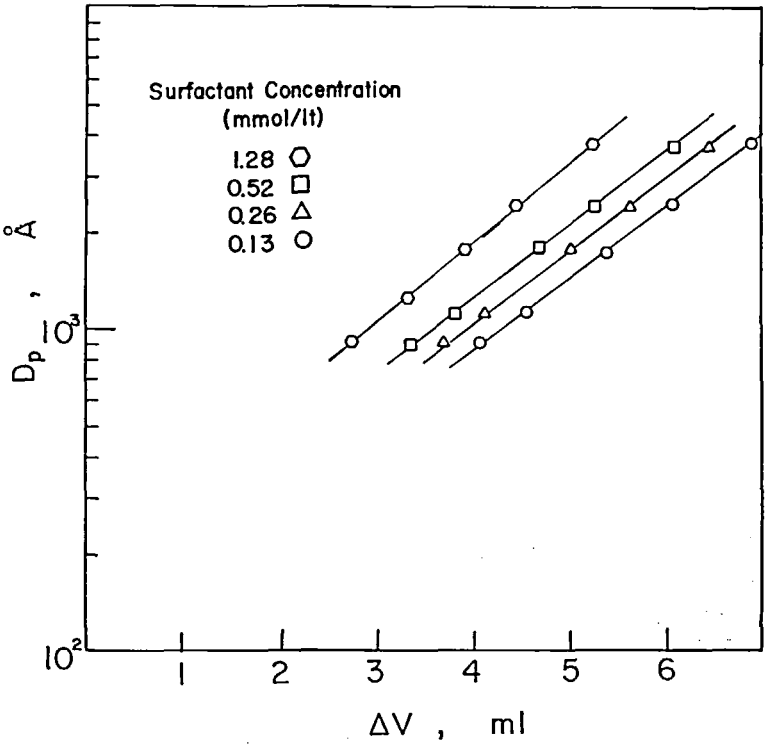


FIGURE 5. Particle diameter vs. elution volume difference for polystyrene latexes at different ionic surfactant concentrations. (From Silebi, C. A. and McHugh, A. J., *AIChE J.*, 24, 204, 1978. With permission.)

On this basis, the separation behavior shows a linear dependence when plotted as log particle diameter vs. ΔV,[25,26,30] an example of which is shown in Figure 5. In this form, the comparison with LEC calibration behavior is striking. At the higher ionic strengths, the linearity is eventually destroyed and, as in the $R_F$ plots, one sees a turn around in the size elution sequence.[25]

An interesting and important feature is the effect of surfactant species and concentration on the separation behavior. Generally, below the critical micelle concentration (CMC) of the surfactant, one sees a behavior pattern precisely the same as that for the low molecular weight ionic species[26,30] as illustrated in Figure 5. This indicates that the surfactant effect can be accounted for by inclusion in the ionic strength definition:

$$I = \frac{1}{2} \sum c_{io} z_i^2 \tag{3}$$

where $c_{io}$ refers to the molar bulk concentration of ionic species i having valence, $z_i$. Similar trends have also been observed in the behavior of $R_F$ when surfactant concentrations greater than the CMC are used. In such cases where only surfactant has been used, Equation 3 has been shown to still be valid for the surfactant provided one includes terms to account for the presence of micellar "macroions".[28] In this latter case, as will be discussed further later, the absence of low molecular weight ionic species appears to also improve the particle recovery characteristics of a given column.

The effect of packing diameter on the $R_F$-$D_P$ (particle diameter) behavior is another feature differentiating HDC from classical chromatography and is illustrated in Figure 6. Whereas the rate of elution of a solute peak is normally independent of the particle size of the stationary phase, here the dependence is dramatic and twofold. First of all, since the resolution of peak separation varies inversely as the slope of the log particle size-ΔV calibration curve,

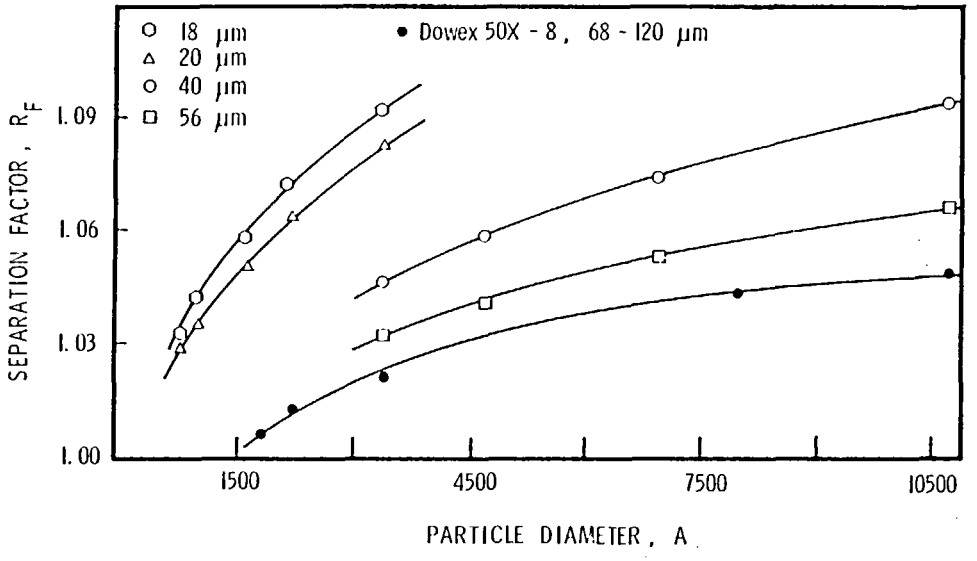


FIGURE 6. Dependence of separation factor on particle diameter and packing diameter.[5,34]



then one sees from Figure 6 that the peak resolution increases with decreased packing size (all other factors held constant). On the other hand, smaller packing diameters decrease the upper size limit of colloidal particles which will elute from the columns.[5] One is thus faced with a trade-off between these counteropposing trends.

As might be expected from its definition, the value of $R_F$ has also been shown to be unaffected by the eluant flow rate over a fairly broad range[26,32] which has important consequences for high performance optimization.

### *3. Calibration and Limits of Operation*

To complete the description of HDC operation, a few words need to be said about calibration and limits of operation. Since one is generally concerned in practical quality control applications, or in particle size distribution determinations with systems other than polystyrene, it becomes important to determine the conditions under which calibration curves obtained for such well-characterized standards can be properly used to determine a particle size. This situation is entirely analogous to the case of macromolecular SEC where universal calibration behavior has been demonstrated on the basis of plots of the product of intrinsic viscosity and molecular weight on a logarithmic scale against elution volume.[33] With particulate systems, at very low eluant ionic strength, one sees universal calibration behavior of particle diameter plotted logarithmically against $\Delta V$ as shown in Figure 7.[28,116]

It is important to emphasize that these observations are specific to so-called "hard" particles, i.e., materials whose glass transition temperatures are greater than room temperature. As the "soft" component of a given latex increases, its recovery in column operation can drop dramatically leading to the suggestion that shear forces may cause particle deformation and possibly increased coalescence.[10,34] It is equally important to emphasize that a practical upper limit exists for the fractionation of particle sizes using a given packing size. The data of Figure 6 include the largest particle sizes for a given packing which will elute from the columns. However, by using a simple column bypass system,[28,34] it has been demonstrated that for a 20-μm diameter packing system, 100% recovery from the columns of a given injection only occurs for particles $\leq$ 200 nm in diameter. In terms of a quantitative recovery (i.e., $\geq$30%), the practical upper limit was found to be 300 nm. Reduced recovery may be due to particle deposition on the packing (which can be avoided by operating under

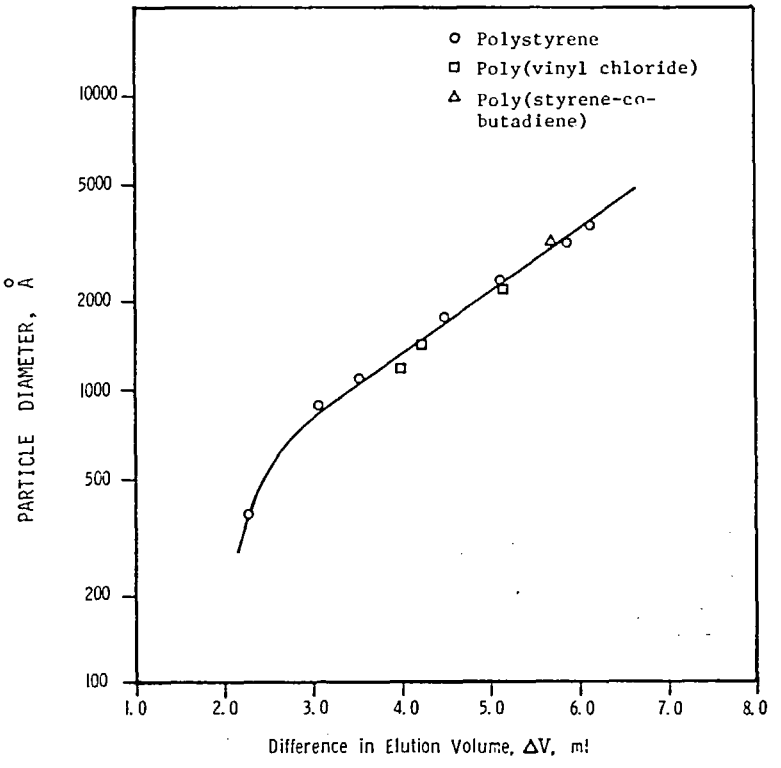


FIGURE 7. HDC universal calibration curve at an eluant ionic strength of 0.00129 AMA. (From Nagy, D. J., Silebi, C. A., and McHugh, A. J., *J. Colloid Interface Sci.*, 79, 264, 1981. With permission.)

conditions of low eluant ionic strength or using surfactant alone as the ionic species),[28] or a filtration effect caused by packing polydispersity.[28] In any case, since complete sample recovery is essential for the calculation of accurate particle size distributions from HDC data, one would be cautioned to operate with as nearly monodisperse a packing system as possible and to not expect quantitative recovery of particles much greater than about one-seventh the packing diameter. Since the data of Figure 6, as already indicated, imply reduced resolution with increasing packing diameter, one concludes that, for quantitative size distribution analysis, packings on the order of 20 μm and particle ranges up to about 350 nm are best suited to HDC.

*4. Mechanism of HDC Separation*

The utility of any analytical technique rests on its accuracy and reproducibility and on the amenability to quantification from a fundamental basis of the essential features of the given method. In the case of HDC, all of the experimental results described in the preceeding sections have been verified independently and are amenable to rationalization as a consequence of the following phenomena: a hydrodynamic effect, electrostatic double layer repulsion, and van der Waals attraction. What follows first is a qualitative description of these phenomena which will be true independently of any specific model for the process. This is then followed by a review of detailed analyses which enable quantification of these phenomena, comparison to data, and prediction of effects.

***a. Qualitative Discussion of Phenomena***

Regardless of the details of a given bed geometry, one expects that in the course of flow through the packing interstices, the eluant will develop a velocity gradient normal to the direction of flow with a maximum velocity somewhere near the center of the interstitial

space, diminishing to zero at the packing surface. As a result of its Brownian motion, a colloidal solute particle will tend to sample all radial positions available to it in the void space and thereby achieve some characteristic mean velocity during its transit through the bed. Due to its finite size, however, one could immediately predict that the approach of the particle center to the packing surface will be limited to a distance equal to its radius. In consequence of this, the particle is, in effect, "excluded" from the slowest moving streamlines and one expects therefore its average velocity will exceed that of the eluant (or more properly an inert marker species) and this trend would increase with particle size. Counterbalancing this increase in average velocity with size is another hydrodynamic phenomenon, that of the so-called "wall effect",[35] whereby the velocity of a particle center lags that of the undisturbed fluid streamline at the same position in the absence of the particle. For a given duct geometry, this effect tends to increase as the ratio of the particle to duct radius and consequently one would eventually expect a reversal to occur in the particle residence time trend. This effect is of some importance and leads to the requirement of the assumption of a bed geometry for its quantitative analysis.

The second-mentioned feature, that of double layer repulsion, has to do with the expected electrostatic interaction between the electrical double layers of the colloidal particle and packing surfaces as the particles approach the packing. The double layer for latex particles results from fixed anionic surface charges (such as sulfate end groups) as well as adsorbed surfactant. In the case of copolymer packing, one has a high fixed density of strong anionic sites, and surfactant adsorption in the case of other systems[5] can explain the packing double layer behavior. In any case, since an increase in double layer repulsion with decreasing eluant ionic strength is well understood and expected,[36] one can rationalize the trend of increased separation factor, since under such conditions particles would be repelled into the faster moving core of the eluant stream.



London-van der Waals attraction forces between the latex particle and packing would also be expected, especially at higher ionic strengths where reduced double layer repulsion allows a closer approach of the two surfaces. Since the attractive force increases with reduced separation distance between the surfaces,[36] one expects under these conditions that the particle will tend to spend greater amounts of time on the slower moving streamlines near the packing (where the wall effect is also greater) and hence suffer a turn around in its average residence time ($R_F$) behavior.

### *b. Bed Capillary Tube Model for HDC*

The incorporation of these effects in terms of a quantitative model for the HDC separation process has been the subject of a number of publications.[24-26,28,30,37,38] In all but one[38] the bed interstices have been modeled on the basis of the equivalent capillary model, basically as envisaged in the earlier HDC approach to size exclusion chromatography.[12-14]

In general, regardless of the assumed flow geometry, the volumetric flow rate, q, associated with a solute species i, marker or colloid, in transit through the bed will be given by:[26]

$$q = \int_{A_i} v_i P \, dA \tag{4}$$

where P represents the probability that i will occupy the given cross section; $v_i$ is the streamline velocity of species i; and $A_i$ represents the flow area accessible to the solute. Owing then to either the finite size of the particle or ionic force field effects (or both), the bed cross section available for flow will, in effect, be less than the interstitial void space. One therefore obtains from Equation 4 for the particle, p, and marker species m, the expression for $R_F$.[26]

$$R_F = \frac{\langle v_p \rangle}{\langle v_m \rangle} \tag{5}$$

In Equation 5, the brackets imply area averaging from Equation 4.

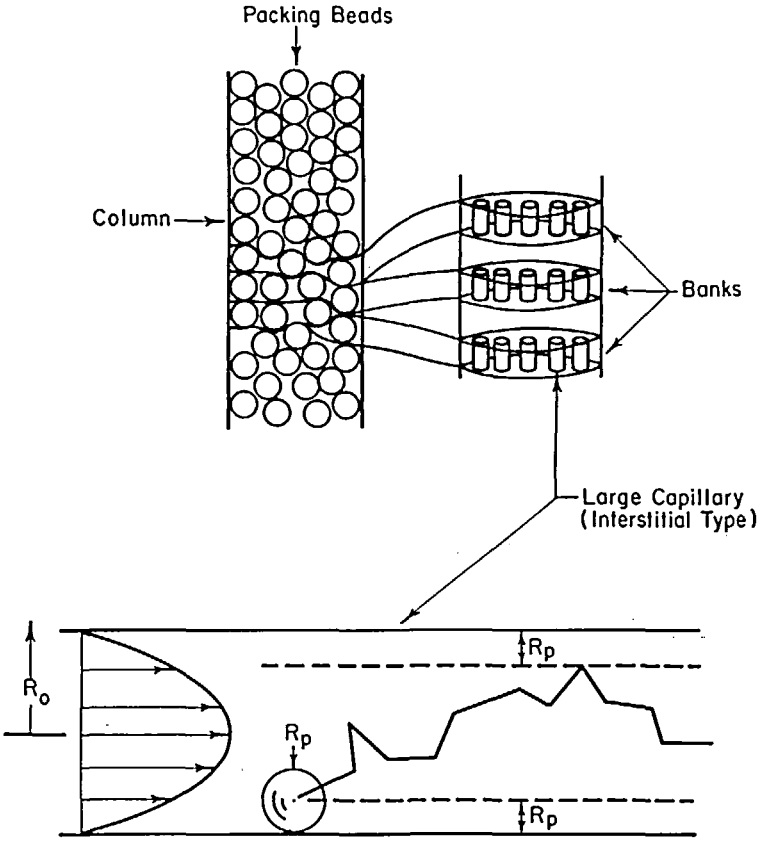


FIGURE 8. Diagrammatic representation of the parallel capillary bed model (top) and illustration of particle trajectory in a typical tube (bottom).



A very complete treatment of the transport of a colloidal solute in a capillary tube geometry has been given by Brenner and Gaydos.[39] In the formalism of chromatography rate theory analysis, one generally starts with the microscopic diffusion equation for the solute and in order to eliminate the problem of attempting to formulate the boundary conditions for the complicated geometry, carries out an appropriate averaging process to obtain the so-called pseudocontinuum[40] or volume-averaged rate equations for the column.[41-43] In the case of a system consisting of charged, noninteracting solute particles, the appropriate starting point is the diffusion equation for the probability density, $P(\underset{\sim}{R},t|\underset{\sim}{R}')$ that a given particle situated at $\underset{\sim}{R}'$ at time $t = 0$ will be at some point $\underset{\sim}{R}'$ at time t:[39]

$$\frac{\partial p}{\partial t} + \underset{\sim}{\nabla}\cdot[P\underset{\sim}{v}_p - \underset{\sim}{D}\cdot\underset{\sim}{\nabla}P - P\underset{\sim}{M}\cdot\underset{\sim}{\nabla}\phi] = 0 \qquad (6)$$

In Equation 6, the diffusivity $\underset{\sim}{D}'$ and mobility $\underset{\sim}{M}'$ are dyadics whose positional dependence is a consequence of the hydrodynamic wall effect; $\phi$ is the total potential energy of interaction between the particle and wall surfaces; k is the Boltzmann constant; and T is the temperature. At low concentrations, P is replaced by the number concentration, C.[39] Conversion of Equation 6 to a volume-averaged or pseudocontinuum form for a packed bed is not so straight forward an operation.[44-46] The approaches taken to modeling HDC have all, in effect, replaced Equation 6 with area-averaged mean fluxes or equivalently, Equation 5, in which the cross section of the bed has been modeled as a parallel bank of equisized capillaries as pictured by Di Marzio and Guttman[12] and shown in Figure 8.

In such a case, by assuming the radial concentration distribution in the capillary tube has equilibrated (i.e., the particle has been in transit for several diffusion times,[26,39] hence the radial flux is zero), the area-averaged equation for the solute species, i, becomes[39]

$$\frac{\partial C_{m,i}}{\partial t} + \langle v_i \rangle \frac{\partial C_{m,i}}{\partial Z} = \bar{D}^* \cdot \frac{\partial^2 C_{m,i}}{\partial Z^2} \tag{7}$$

In Equation 7, $C_{m,i}$ represents the averaged concentration of species i, particle or marker, in the mobile or eluant phase; $\bar{D}^*$ is the phenomenological dispersion coefficient given by Brenner and Gaydos;[39] and $\langle v_i \rangle$ is the solute average velocity which for the given species is

$$\langle v_i \rangle = \frac{\int_0^{R_o - R_i} v_i(r)\, e^{-\phi/kT}\, r\, dr}{\int_0^{R_o - R_i} e^{-\phi/kT}\, r\, dr} \tag{8}$$

In Equation 8, $R_i$ is the solute particle radius.[26] According to the earlier discussion, for the particle species one should expect $\phi$ to contain terms for the double layer repulsion, $\phi_{DL}$, and van der Waals attraction, $\phi_{VW}$, however for completeness one could also include a term for short-range Born repulsion,[15] $\phi_B$, and surfactant (or other macromolecular adsorbed species) steric repulsion,[30] $\phi_{ST}$. Thus by the standard linear additivity assumption:

$$\phi = \phi_{DL} + \phi_{VW} + \phi_B + \phi_{ST} \tag{9}$$

For the particle species, Equation 8 requires explicit accounting of the hydrodynamic wall affect in the velocity term in the integral and in the definition of the terms associated with the phenomenological dispersion coefficient $\bar{D}^*$.[39] Solution of Equation 7, subject to the standard chromatography boundary conditions,[42,43] would, in principle, give expressions for the output chromatogram. However, as an approximation suitable for the analysis of the average residence time, $\bar{D}^*$ can be set equal to zero, in which case one obtains immediately from the moments of the output chromatogram the mean residence time, $\theta_i$, for the particle or marker, at the column outlet (Z = L):

$$\theta_i = \frac{L}{\langle v_i \rangle} \tag{10}$$

Since the elution volume $V_i$ is just $q\theta_i$, one obtains from Equations 1 and 10 the expression given by Equation 5 where now the meaning of the average velocity terms for the capillary model is explicit.

### *c. Quantitative Evaluation of $R_F$*

Evaluation of Equations 5, 8, and 9 enables quantitative prediction of the separation factor-particle size behavior. The particle streamline velocity, $v_p(r)$ is given by:[35]

$$v_p(r) = v_o \left(1 - \frac{r^2}{R_o^2}\right) - \gamma\, v_o \left(\frac{R_p}{R_o}\right)^2 \tag{11}$$

where $\gamma$ is the wall-effect parameter; $R_p$ is the particle radius; and the first term is the familiar laminar flow profile for the eluant free stream velocity having a centerline value, $v_o$. Expressions for $\gamma$ can be written as[26]

$$\gamma = 2/3\,(1 + 3\, r/R_o) \quad \text{core region} \tag{12a}$$

$$\gamma = 5/8\, \frac{R_p/R_o}{(1 - r/R_o)^2} \quad \text{wall region} \tag{12b}$$

$$\gamma = \frac{R_o^2}{R_p^2}\left[1 - \frac{0.7431}{0.6376 - 0.2\,\ell n\left(\frac{R_o}{R_p} - \frac{r}{R_p} - 1\right)}\right] + \qquad (12c)^*$$

$(1 - r^2/R_o^2)$ close to the wall

In order to treat the double layer repulsion and van der Waals attraction, one normally uses expressions for the interaction of a sphere (particle) and plane (packing) since the relative radii ratio is generally less than 1/40. Approximate expressions developed by Bell et al.[47] have been used[26,28,30] since these cover the range from small to large particle-wall separations (needed in Equation 8), as well as a wide range of surface potentials. These generalized forms for a symmetric 1-1 electrolyte are

$$\phi_{DL} = \epsilon\left(\frac{kT}{e}\right)^2 Y_1 Y_2 R_p \exp(-\kappa a) \qquad (13a)$$

$$Y_1 = 4 \tanh\left(\frac{\Phi_1}{4}\right) \qquad (13b)$$

$$Y_2 = Y_2(\Phi_2, \kappa R_p) \qquad (13c)$$

$$\Phi_i = \frac{e\,\psi_{oi}}{kT} \qquad (13d)$$

in which $\epsilon$ is the eluant dielectric constant; $\Phi_i$ are the dimensionless surface potentials; $\psi_{oi}$, for the packing, 1, or particle, 2; a is the separation distance between the wall and packing surface; and $\kappa$ is the familiar reciprical Debye double layer thickness,[36] which is given in terms of the protonic charge, e, and the ionic strength as:

$$\kappa = \sqrt{\frac{8\pi e^2 I}{\epsilon kT}} \qquad (14)$$

The function $Y_2$ has the following analytical form for symmetic 1-1 electrolytes under conditions such that $\kappa R_p \geq 5$:

$$Y_2 = 4 \tanh(\Phi_2/4) \qquad (15)$$

For small particle sizes and low ionic strengths where $\kappa R_p < 5$, one needs the tabular values[47] which are obtained from the numerical solution of the nonlinear Poisson equation.[48] The latex surface potential depends on the surface charge density, $\sigma_s$, and ionic concentration, $c_o$, in the eluant phase, and for symmetric electrolytes is[49]

$$\sigma_s = \sqrt{\frac{2\epsilon\, kT\, c_o}{\pi}} \sinh\left(\frac{z\, e\, \psi_{o2}}{2\, kT}\right) \qquad (16)$$

A generalized form of Equation 16 for a solution containing several electrolytes has been given by Silebi.[26,50] Equation 16 suffers from the same restriction on $\kappa R_p$ as Equation 15, thus numerical evaluation of the surface charge density may be required. The total surface charge density in the presence of the surfactant can be evaluated from measurement of the zeta potential at given total ionic strength.[51]

Equations 13 and 16 represent the most rigorous treatment of $\phi_{DL}$ and were used in the calculations to be discussed.[26] However, the general trends can also be described by the

* Equation 12c is the corrected form of Equation 8c in Reference 26.

more simplified forms used by some authors.[15,37,38] More recently[111] it has been demonstrated that an approximated form of the spherical Poisson-Boltzmann equation yields analytic expressions for the surface charge density which are simple in form and yield remarkably accurate results in the parameter range needed for the double layer repulsion and surface charge density/surface potential relationships. The appropriate forms are[111]

$$Y_2 = 8 \tanh\left(\frac{\Phi_2}{4}\right) \frac{1}{1 + \left[1 - \frac{2\kappa R_p + 1}{(\kappa R_p + 1)^2} \tanh^2\left(\frac{\Phi_2}{4}\right)\right]^{1/2}} \tag{17}$$

and

$$\sigma_s = 2\left(\frac{\epsilon\,\kappa\,kT}{4e\pi}\right) \sinh\left(\frac{\Phi_2}{2}\right) \left(1 + \frac{2}{\kappa R_p \cosh^2\left(\frac{\Phi_2}{4}\right)} + \frac{8\,\ell n\,[\cosh(\Phi_2/4)]}{\kappa^2 R_p^2 \sinh^2(\Phi_2/2)}\right)^{1/2} \tag{18}$$

They eliminate the need for use of the numerical calculations.

The van der Waals attractive energy, $\phi_{VW}$, can be evaluated from the expression developed by Clayfield and Lumb.[52] Since a discontinuity occurs in the first derivative at the transition between the region of small separations where the retardation effect is negligible and the region of large separations where retardations must be considered, one has to evaluate somewhat cumbersome expressions[26] or use less accurate forms.[15,37,38] A recently published approximate form,[53] which is much simpler and yields accurate results for $\phi_{VW} < 0.1\ A_H$, where $A_H$ is the Hamaker constant, is

$$\phi_{VW} = -\frac{A_H R_p}{6a} \frac{1}{1 + 14a/\lambda} \tag{19}$$

In Equation 19, $\lambda$ is the characteristic wavelength of the dispersion interaction.

Since the Born repulsive forces are very short range,[15] they turn out to be of negligible importance.[26] Also, since low molecular weight anionic surfactants have been used, steric repulsion has not been considered important, although an approximate expression is available.[30]

With regard to the marker species, for a noninteracting trace, $\langle v_m \rangle$ would simply be one half the capillary centerline velocity.[54] For the ionic species ($Cr_2O_7^=$) one can assume the Born and London-van der Waals terms would be negligible; hence taking the limiting forms of Equations 13 as $R_p \rightarrow O$, one gets $Y_1 \rightarrow \Phi_1$ and $Y_2 \rightarrow 2e^2/kT\epsilon R_p$. Thus Equation 8 gives:[26]

$$\langle v_m \rangle = \frac{\int_0^{R_o} v_o\left(1 - \frac{r_2}{R_o^2}\right) \exp\left[\frac{-2e\,\psi_{o1}}{kT} \exp(-\kappa a)\right] r\,dr}{\int_0^{R_o} \exp\left[\frac{-2e\,\psi_{o1}}{kT} \exp(-\kappa a)\right] r\,dr} \tag{20}$$

Comparison of Equation 20 to the experimental data reported by Small[5] for the ionic strength effect on the marker peak shows this approach can explain the effect of lowered $V_m$ alluded to earlier. Equations 8, 11 to 13, 16, and 20 represent then the complete description of the HDC separation factor $R_F$.

*5. Comparison of the HDC Model to Experiment*

Typical values of the Hamaker constant for polymer latex systems in water[55] are listed in Table 3. The range for $A_H$, evaluated by different experimental and theoretical methods is seen to be typically 0.005 to 0.30 perg. Values of the zeta potential (approximated as the surface potential) are generally in the range of 20 to 150 mV and display an ionic strength

**Table 3**
**VALUES OF THE HAMAKER CONSTANT FOR TYPICAL LATEXES IN WATER[55]**

| Latex type | Range of Hamaker constant (perg) |
|---|---|
| Polystyrene | 0.01—0.1 |
| Poly(vinyl chloride) | 0.05—0.2 |
| Poly(methyl methacrylate) | 0.07—0.7 |
| Poly(vinyl acetate) | 0.04—0.4 |
| Polytetrafluoroethylene | 0.002—0.01 |
| Polyethylene | 0.10 |
| Styrene-butadiene | 0.02—0.20 |
| Polystyrene-acrylonitrile | 0.02—0.10 |

dependence associated with a constant surface charge.[51] The equivalent capillary radius, $R_o$, is obtained directly from a knowledge of the packing diameter, $D_{PK}$, and bed porosity, $\epsilon_v$, in terms of the hydraulic radius:[54]

$$R_o = \frac{D_{PK}}{3} \frac{\epsilon_v}{1 - \epsilon_v} \tag{21}$$

From the data of Small[5] for 20-μm packing, this gives values of $R_o$ equal to 3.72 μm, which was used in the result to be discussed.

Figures 9 and 10 show the effects on the separation factor-particle diameter relationship of ionic strength in the eluant phase. At low ionic strengths (≤0.001 *M*) one sees that the separation characteristics are independent of the Hamaker constant, i.e., particle chemistry, and are therefore dominated by hydrodynamic effects with electrostatic repulsion superposed. Similar results are shown in other calculations[37,38] along with the same effects observed by varying the surface potential.[26,30,50] These results clearly indicate the nature of the universal calibration conditions established experimentally (Figure 7).

Figure 10 shows that at relatively high ionic strength, 0.1 *M*, the separation behavior becomes highly sensitive to material parameters indicating that separation will be strongly influenced by particle chemistry (i.e., Hamaker constant and surface potential). In other words, since, as a result of the reduced double layer repulsion, particles can approach closer to the packing surface during their transit through the bed, their velocity will tend on average to be lower, with the precise "weighted average" position now strongly sensitive to $\phi_{VW}$. In addition to showing that for a given latex system particle separation may begin to reverse itself at these high ionic strengths, these calculations also illustrate an alternate and important application, namely that of separating equisized particles of different chemistry. Such chromatographic separation has been reported[56] wherein mixtures of polystyrene and poly(methyl methacrylate) latexes of nearly the same diameter (approximately 254 nm) were separated at the high ionic strength of 0.4 *M*. Percent recoveries were not reported, however one would assume that a more concentrated injection would be needed since recoveries at high ionic strength conditions have been shown to be low.[28] Alternately, these results suggest the applicability of potential barrier chromatography[15,16] discussed earlier, since in this realm adsorption-desorption kinetics may begin to dominate the process. The results regarding recovery using surfactants[28] would suggest the use of nonionic systems [such as poly(ethylene oxide) or poly (ethylene glycol)] to help stabilize against irreversible flocculation.

Figures 11 and 12 show a comparison between the experimental results of Small[5] and those calculated by the HDC capillary model. The total ionic strength computed from Equation 3 for the concentration in these figures has been reduced to total equivalent NaCl

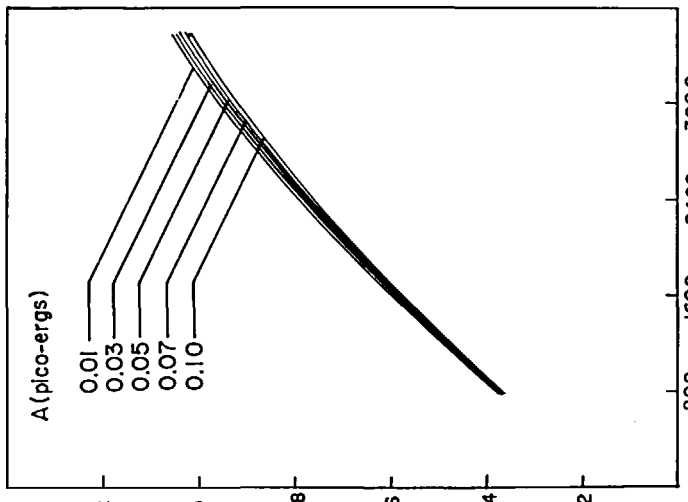


FIGURE 9. Capillary bed model computation showing the $R_F$-particle diameter behavior at a low ionic strength, 0.001 *M*. $\psi_{o1}$ = 90 mV; $\Psi_{o2}$ = 30 mV; $\epsilon$ = 74.3; T = 300°K. (From Silebi, C. A. and McHugh, A. J., *AIChE J.*, 24, 204, 1978. With permission.)

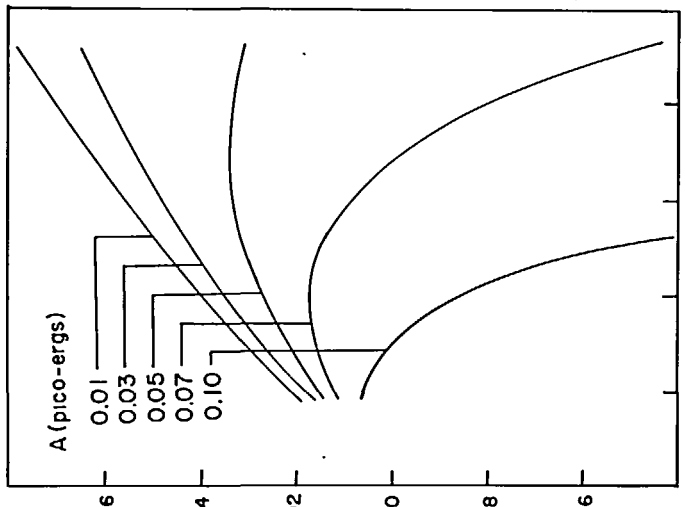


FIGURE 10. Capillary bed model computation showing the $R_F$-particle diameter behavior at high ionic strength, 0.1 *M*. (From Silebi, C. A. and McHugh, A. J., *AIChE J.*, 24, 204, 1978. With permission.)

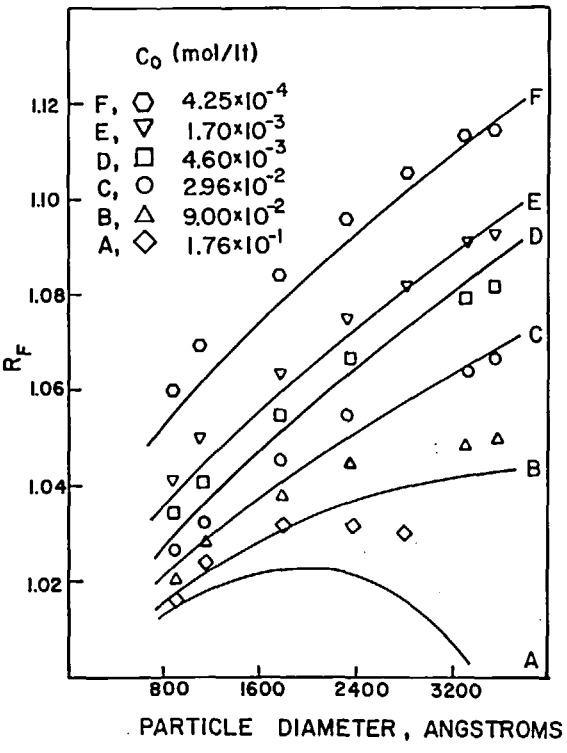


FIGURE 11. Comparison between HDC model and polystyrene data of Small.[5] $A_H$ = 0.05 perg; $\psi_{o2}$ = 30 mV; $\sigma_s$ = 1.5 × $10^4$ stc/cm². (From Silebi, C. A. and McHugh, A. J., *AIChE J.*, 24, 204, 1978. With permission.)

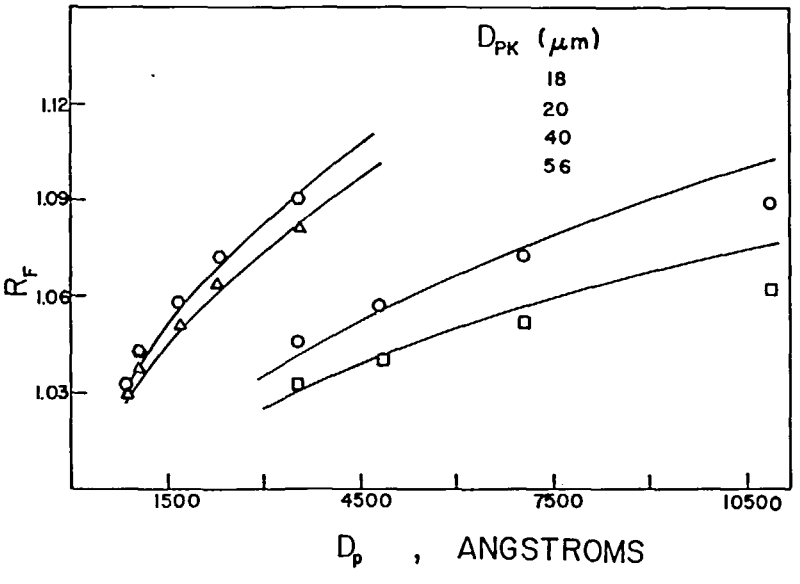


FIGURE 12. Comparison between predicted and measured $R_F$-particle diameter behavior for various packing sizes. $A_H$ = 0.05 perg; $\psi_{o1}$ = 125 mV; $\psi_{o2}$ = 30 mV; 4.6 × $10^{-3}$ *M* sodium chloride. (From Silebi, C. A. and McHugh, A. J., *AIChE J.*, 24, 204, 1978. With permission.)

with the surfactant included since it is present below its CMC. This reinforces the conclusion that the surfactant at concentrations below the CMC behaves merely as another ionic species. It is important to note that the strikingly good fit seen in both plots is a consequence of a zero-free parameter calculation and therefore lends strong support to the accuracy of the capillary model. Similar results were reported in other calculations.[37,38] The capillary model also gave a similar excellent fit to separation factor data obtained on another HDC column system in which surfactant alone was used as the ionic species.[28] For concentrations above the CMC, an addition to the ionic strength was made to include the total charge expected for the anionic micelles.[57] Otherwise, the parameters used for the calculations were the same as those used in Figures 11 and 12.

As a final note regarding the assumptions of the HDC model, the effect of bed length (i.e., number of columns) has been shown to be zero.[34] It is important to note that the relative rate of particle transport, as expressed by Equation 5, should indeed be independent of bed length. However, as will be discussed, the specific resolution or separation efficiency of the HDC system depends, in addition, on the axial dispersion behavior which will be a function of bed volume, length, packing size, and eluant flow rate.

## B. Porous Packing Chromatography

The application of porous packing or liquid size exclusion chromatography to particle size analysis has been stimulated by the early work of Krebs and Wunderlich,[4] who demonstrated that polystyrene and poly(methyl methacrylate) latices could be fractionated using columns packed with a silica gel having pore sizes ranging from 50 to 5000 nm. The observed linearity of their calibration curve of log (particle diameter) vs. elution volume was strikingly similar to that seen for SEC of macromolecules and suggested the method could be used for particle size analysis. Since then a number of studies have been published in which a range of packing sizes and types have been used to fractionate various polymer latex systems.[17,18,32,58-62] In this section, a description of the details of the porous packing experiment will be given, followed by a discussion of the separation characteristics and a review of the quantitative mechanisms proposed to explain the process. A good deal of the methodology parallels that of the HDC experiment.



### *1. Experimental Conditions*

The basic setup of the porous packing chromatography systems is the same as shown in Figure 2 for HDC. The ranges of polymer latex systems, particle sizes, and eluant conditions studied are also virtually the same as those for HDC as listed in Table 2, except that a number of studies have also investigated the separation characteristics of colloidal silica particles[17,18,59] and in some cases, *in situ* polymerized systems such as poly(vinyl acetate)[18] and various other copolymer latex systems have been investigated.[17,59] The surfactant species and ionic species have been added to the eluant phase for basically the same reasons of stabilization as is done in HDC but also, as will be shown, to attempt to further control particle permeation into the porous packing phase. The range of eluant flow rates and operating conditions have been otherwise much the same as HDC with either refractive index or turbidity as the signal measurement.

The key and critical difference, of course, has been with the use of porous packings in a range of pore diameters and packing sizes. Table 4 shows a summary of the packing systems which have been studied. Generally several columns have been used in series, each with a different packing pore size range, with the idea having been to mimic the operating conditions known to be optimal for macromolecular SEC.[6] A logical expectation has been that superposing a porous phase-mobile phase size exclusion partitioning would exacerbate the size separation, all other things being equal. To an extent, this has been the case. Although trends in the data give a clear indication that separation will be enhanced by the

Table 4
SUMMARY OF PACKING SYSTEMS APPLIED TO PARTICLE CHROMATOGRAPHY

| Packing type | Mean pore diameter or range (nm) | Packing size range | Ref. |
|---|---|---|---|
| Porous silica (10,000 Å) | 50—5000 | | 4 |
| Porasil, EX (deactivated porous silica) | 80—150 | 74—125 μm | |
| SIL 5000 porous silica | 300—600 | 74—125 μm | 59 |
| SIL 10000 | 400—1300 | 74—125 μm | 59 |
| Controlled pore glass (CPG) | 50, 100, 150, 200, 250, 300 | 100—400 mesh | 9, 17, 18, 58—62, 64 |
| Fractosil | 490, 1400, 3000 | 120—230 mesh | 9, 18, 58, 62, 64 |
| Bioglass | 100, 150, 250 | 100—200 mesh | 18, 61, 64 |
| Glass | 10, 20—40, 40—80 | 75—125 μm and 120—200 mesh | 18, 61, 64 |

porous phase, conclusions regarding a size separation mechanism and the resolution characteristics are less clear-cut than with HDC.

When considering the porous systems, a distinction between the pore internal volume, $V_i$ (whether stagnant or open flow through), and the interstial void volume, $V_o$, needs to be made. One can define a coefficient k′ to indicate the fraction of the total internal pore volume accessible to a solute particle in terms of the measured elution volume for the particle peak, $V_p$, and $V_o$, as:[32,60,62]

$$V_p = V_o + k' V_i \quad (22)$$

If indeed the separation mechanism were that of SEC, one would expect k′ to range from 0 to 1. In such cases, the considerable attention given in the literature to the mechanistic interpretation of k′ (often written as $K_{SEC}$) and its interpretation as a true equilibrium distribution coefficient, would be germane to the particle chromatography process. For example, mathematical solutions of the rate equations for SEC show Equation 22 as the proper form for the chromatogram first moment[43] and a number of experimental studies (conveniently summarized in Reference 6) corroborate this interpretation of k′ as an equilibrium partition coefficient for flexible macromolecular systems. Obvious similarities with treatments of the size exclusion mechanisms for rigid macromolecules[63] might lead to the expectation that particle chromatography in a porous bed is similarly an equilibrium process. Unfortunately, as will be seen, experiments and models of the particle process are not unambiguous on this point. Significant HDC effects may occur and, in fact, be desirable in the interstitial mobile phase.

*2. Separation Characteristics*

James et al.[59] investigated the fractionation of several latex systems including butadiene copolymers of styrene and acrylonitrile. A fairly complete study (originally disseminated in Reference 58) was carried out by Coll and Fague[17] using various controlled-pore glass (CPG) packings and a set of 5 columns (0.5 cm-ID) with a total length of 6 m. Nominal pore sizes in the respective columns were 300, 200, 200, 100, and 50 nm. The aqueous mobile phase eluting solution was pumped at a fixed flow rate of 0.7 mℓ/min and included various surfactants to control stability and salt ($KNO_3$) to control ionic strength. Detection was by differential refractometry and turbidity. Figure 13 shows the calibration curve obtained at

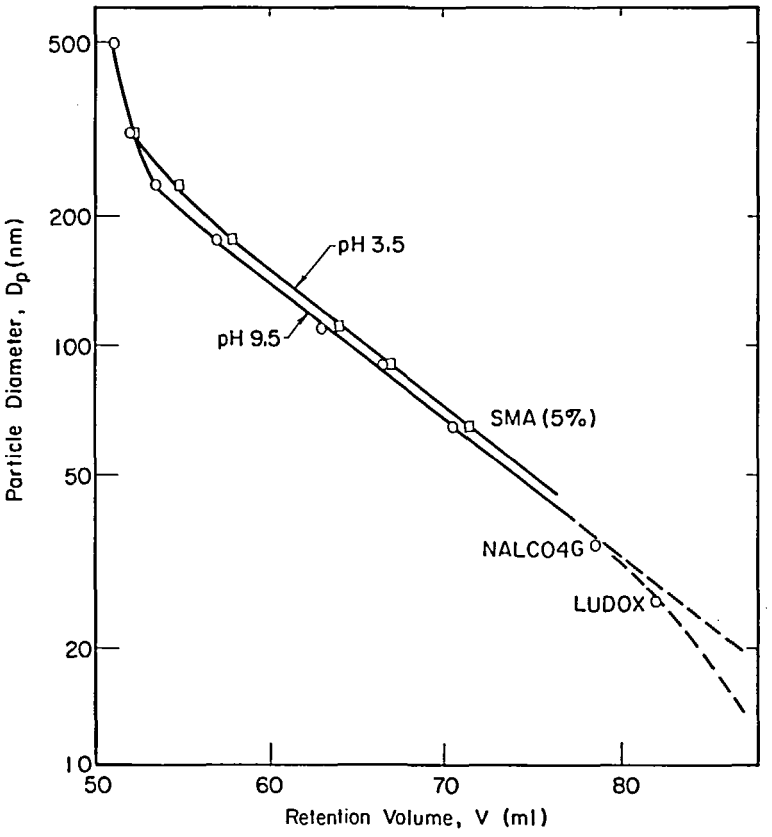


FIGURE 13. Calibration curve obtained at pH = 3.5 and 9.5 with a porous system. (From Coll, H. and Fague, G. R., *J. Colloid Interface Sci.*, 76, 116, 1980. With permission.)

**Table 5**
**LEC DATA OF COLL[17]**

| $D_p$ (Å) | $V_{R,p}$(mℓ) | $R_F$ | k′ |
|---|---|---|---|
| 250[a] | 82.0 | 1.171 | 0.68 |
| 350[a] | 78.5 | 1.223 | 0.60 |
| 640 | 71.4 | 1.345 | 0.44 |
| 910 | 67.0 | 1.433 | 0.34 |
| 1090 | 64.0 | 1.500 | 0.27 |
| 1760 | 58.0 | 1.655 | 0.13 |
| 2340 | 54.8 | 1.752 | 0.06 |
| 3120 | 53.5 | 1.794 | 0.03 |

Colloidal silica.

two different pH values. It bears a striking similarity to a macromolecular SEC calibration plot. The data show a small shift of retention volume with pH suggesting somewhat smaller effective particle diameters, or slightly more spacious pores, at the lower pH.[17] The retention volume data can be converted to $R_F$ values using the total void volume (pore + interstices) of 96 mℓ.[58] These are listed in Table 5 along with values of k′ calculated using an interstitial void volume of 51.2 mℓ.[34] The relationship between $R_F$, k′, and total void volume $V_T$ readily follows from Equations 1 and 22, assuming that $V_T$ is given by the elution volume of the marker species. Thus:

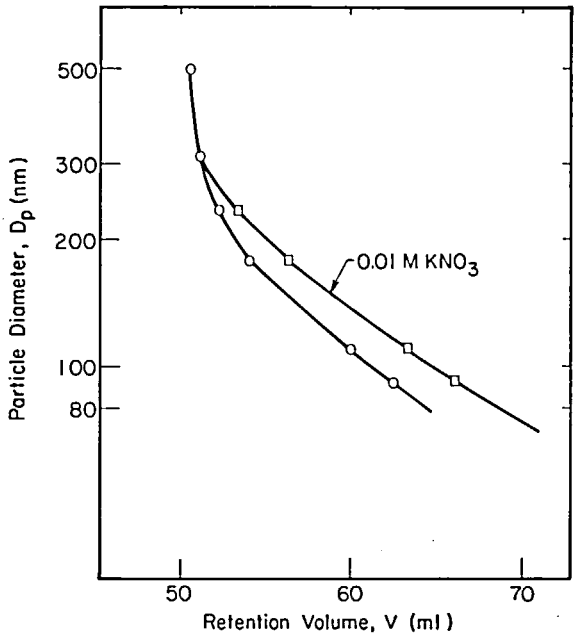


FIGURE 14. Effect of ionic strength on calibration curve with a porous system: (○) 1 gm/lt Aerosol OT; (□) 1 gm/lt Aerosol OT + 0.01 *M* $KNO_3$.(From Coll, H. and Fague, G. R., *J. Colloid Interface Sci.*, 76, 116, 1980. With permission.)

$$k' = (1/R_F - 1)\frac{V_T}{V_p} + 1 \qquad (23)$$

The data show a wide range of k′ values whose magnitude drops dramatically for particles greater than 100 nm. One would expect that particles larger than this would be excluded completely from the porous matrix. Thus the steep linear upturn in the calibration curve of Figure 13 corresponds to an HDC region. Qualitatively, it would appear therefore that the milder slope in the exclusion region and larger $R_F$ values indicate an improvement in resolution.[25] However, the increased $R_F$ values are largely a reflection of the fact that the marker species can sample essentially the entire void volume while the particle is being largely excluded from the pores.[62] In addition, peak broadening observed for the polystyrene standards indicated that the specific resolution was not as good as observed for macromolecular SEC.[17]

The effect of mobile phase ionic strength on the calibration curve was also investigated by the addition of $KNO_3$ to the eluant. Figure 14 indicates that the addition of salt implies reduced double layer repulsion and therefore an increase in accessible pore volume.[17] Using a nonionic surfactant (Triton X-100) resulted in latex particles emerging from the columns near $V_o$ indicating virtual exclusion of the particles from the porous phase. Thus, as in HDC, ionic strength plays a major role in the separation process and in this case may also be controlling a shift between the relative amounts of HDC- and LEC-type fractionation. Percent recovery data were not reported in these studies, however, skewing of the chromatographic peaks was noted,[17,58] possibly indicating particle entrapment in the pore phase.

The system investigated by Singh and Hamielec[18] employed a much wider range of pore sizes (10 to 3000 nm) and was used as an off-line monitor to follow particle growth in an emulsion polymerization. A more extensive series of studies of the resolution characteristics was also carried out.[61,64] Combinations of column packed with a range of materials (indicated in the listing of Table 4) were used. Eluant chemistries were similar to the previously mentioned study; however, a range of flow rates (0.94 to 7.5 mℓ/min) was also studied.

Linear calibration curves (log diameter vs. retention volume) were obtained for the various column combinations and latex particle types (polystyrene, polyvinylacetate, styrene-acrylic acid copolymer, butadiene-acrylonitrile copolymer latices, and colloidal silica) in eluant containing 1 g/ℓ aerosol OT and 1 g/ℓ $KNO_3$ (total ionic strength of 12.6 m*M*). The shape of the curve was the same as those shown in Figure 13 and the superposition of latex types clearly indicated universal calibration behavior such as seen in HDC.[28] Similar to HDC, the corrected calibration curves were also essentially independent of flow rate.[64] The later study[61] indicated the importance of individual column calibration. Discussions of the dispersion behavior will be delayed to a later section.

Extensive studies of the separation characteristics of small and large pore packing systems have been reported.[9,32,60,62] In the first instance,[9,32,62] stainless-steel columns (1/16 in. O.D. capillary tubing) were packed with either a series of the CPG materials ranging in pore size from 50 to 1000 nm or one column packed with a large pore diameter (2.5 μm) Fractosil system. Mobile phase chemistries included surfactant only as the ionic species. Figure 15 shows the effect of different CPG packing distributions on the $R_F$-particle diameter behavior at a low ionic strength (5.2 m*M*). Column set I comprised three columns in series with packing pore diameters of 50, 100, and 200 nm, respectively; set II consisted of three columns with packing diameters of 100, 200, and 300, nm respectively; and set III was a single column packed with material having a 1000-nm pore size. Column sets I and II indicate a sharp distinction between two regions, one at small particle diameter where the steeper slope corresponds to particle penetration in the pore matrix and the flatter region to a more purely HDC behavior. This behavior is analogous to the double slopes seen on the retention volume calibration curve of Figure 13. Since resolution varies as the slope of the $R_F$ curve, steeper slopes in the LEC region indicate higher resolution, whereas the reverse holds true for the slope on a ΔV plot. These data indicate that significant pore penetration by the solute particles only occurs for pore diameters on the order of two to three times that of the particles,[62] similar to observations made with macromolecular systems.[65] Balancing the improved resolution implied in Figure 15 for the smaller pore systems was the detrimental effect of poor particle recovery. Material balances obtained by comparing turbidity peaks using a column bypass line showed that recoveries of particles greater than 100 nm in diameter were less than 50%. Increased skewness of the chromatogram peaks with increasing particle size further indicated entrapment of particles in the porous phase as the most probable explanation.[62] On the other hand, particle recoveries with the 1-μm system were improved, and as a consequence of greater particle penetration of the porous matrix, a single curve results with $R_F$ values nearer to those of HDC, since the artificial disparity between $V_m$ and $V_p$ has been reduced. Similar trends were observed in the study by Johnston et al.[60]

An interesting correspondence with the ionic strength behavior seen in HDC was found with the 2.5-μm pore diameter Fractosil system.[32,62] Comparison of k′ values obtained from Equation 22 for column set II and a single glass column packed with Fractosil is given in Table 6. They illustrate that a significant increase in pore penetration by all particles occurs with the larger pore system. Figure 16 shows the $R_F$-particle diameter behavior for this system over a range of eluant ionic strengths where the striking similarity to HDC behavior (Figure 4) is apparent. Since eluant ionic strengths were controlled with surfactant, in some cases concentrations above the CMC were used. In such cases, the total ionic strength was calculated using Equation 3 and the equivalent micelle charge[32] as discussed earlier. A useful practical observation was the improvement in recovery seen under such circumstances.[62] Although slopes of the calibration curves for these porous systems (CPG, Fractosil etc.) all appear to show increased resolution of peak separation[32] over an HDC system, increased axial dispersion (band broadening) in porous systems leads ultimately to reduced resolution as will be discussed later. With the larger pore system independence of the separation factor with flow rate was also observed,[32] similar to the earlier mentioned study.[64]

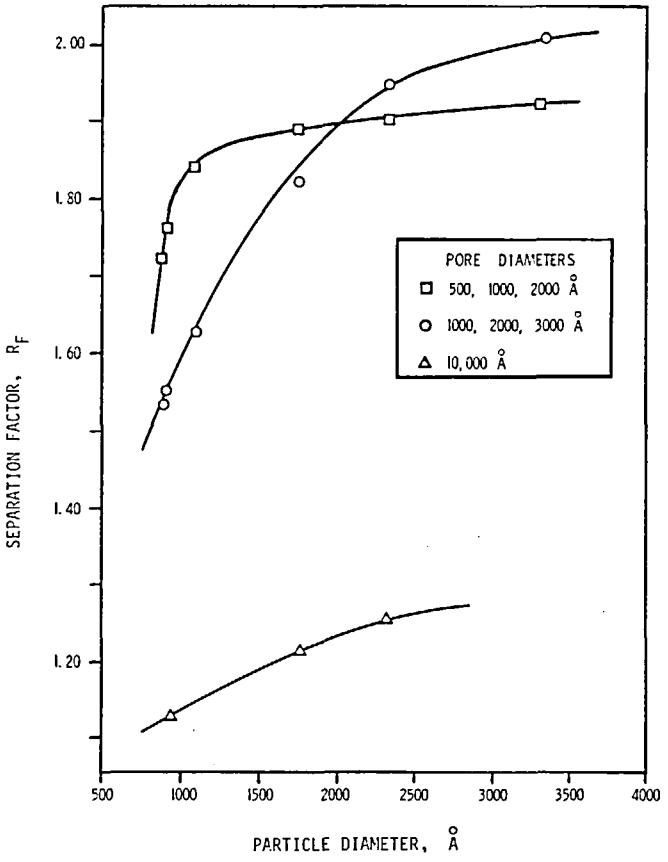


FIGURE 15. Effect of pore size distribution on $R_F$ for polystyrene latices using various LEC packings at 0.0052 *M* AMA. (From McHugh, A. J., Nagy, D. J., and Silebi, C. A., *Size Exclusion Chromatography (GPC)*, ACS Symp. Ser. 138, Provder, T., Ed., American Chemical Society, Washington, D.C., 1980, 1. With permission.)

## Table 6
## k′ FACTORS FOR CPG AND FRACTOSIL PACKINGS

| $D_P$ (Å) | CPG[a] | Fractosil[b] |
|---|---|---|
| $Na_2Cr_2O_7$ | 1.00 | 1.00 |
| 880 | 0.25 | 0.84 |
| 910 | 0.23 | 0.83 |
| 1090 | 0.16 | 0.81 |
| 1760 | 0.02 | 0.75 |
| 2340 | 0.02 to 0 | 0.69 |
| 3570 | 0 | 0.59 |

[a] Three columns: pore sizes of 1000, 2000 and 3000 Å (set II).
[b] One column: pore size of 25,000 Å.

From McHugh, A. J., Nagy, D. J., and Silebi, C. A., in *Size Exclusion Chromatography*, ACS Symp. Ser. 138, Provder, T., Ed., American Chemical Society, Washington, D.C., 1980, 1. With permission.

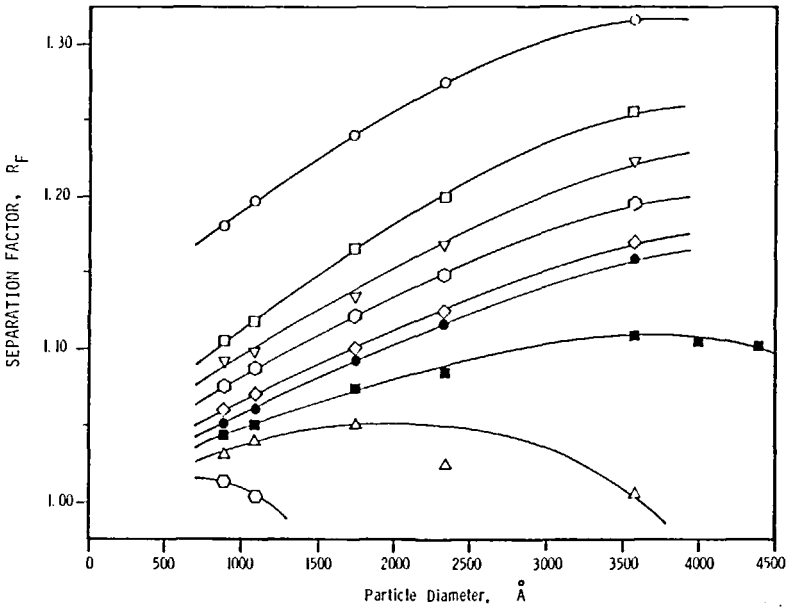


FIGURE 16. $R_F$-particle diameterdata for polystyrene latices for a large pore diameter (2.5 μm) Fractosil system. Total ionic strengths in the eluant phase: (○) 0.00022 *M* SLS; (□) 0.00055 *M* SLS; (▽) 0.00103 *M* SLS; (◇) 0.00129 *M* AMA; (◇) 0.00515 *M* AMA; (●) 0.0101 *M* AMA; (■) 0.0210 *M* SLS (I = 0.053 *M*); (△) 0.035 *M* SLS (I = 0.101 *M*); (<>) 0.105 *M* SLS (I = 0.342 *M*). Quantities in parentheses are total ionic strengths. (From McHugh, A. J., Nagy, D. J., and Silebi, C. A., *Size Exclusion Chromatography (GPC)*, ACS Symp. Ser. 138, Provder, T., Ed., American Chemical Society, Washington, D.C., 1980, 1. With permission.)

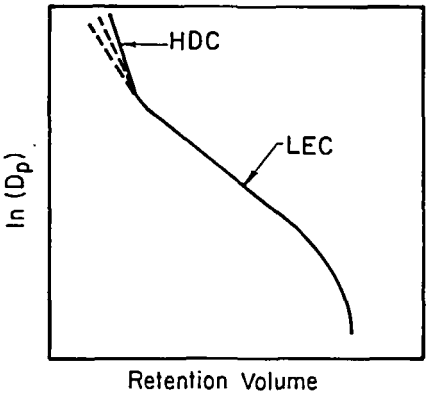


FIGURE 17. General calibration curve for porous packing system illustrating relative ranges of HDC and LEC. Dotted lines represent decreasing packing size in HDC. (From McHugh, A. J., Silebi, C., Poehlein, G. W., and Vanderhoff, J. W., *J. Colloid Interface Sci.*, 4, 549, 1976. With permission.)

### *3. Separation Mechanisms in Porous Packing Systems*

#### *a. Porous Flow-Through Model*

From the data reviewed, it is clear that addition of the porous matrix complicates the possibilities regarding a size separation mechanism. It would seem that depending upon: (1) the relative size and connectivity of the porous matrix regions and the packing interstices, (2) the particle size, and (3) potential force field effects, the controlling separation mechanism could be pore partitioning, HDC, or a combination of both. A schematic illustration of a general calibration curve is illustrated in Figure 17 whereby one might reasonably argue that

for particles large enough to be excluded from the porous matrix, the separation mechanism should be HDC as described in the earlier sections. In the region of pore penetration, one would expect separation behavior similar to SEC, however, the data of Figure 16 display trends strongly suggestive of HDC. Although the dominant mechanism for macromolecular SEC is the exclusion process,[6] it has in fact been shown that some separation due to the HDC mechanism can also occur.[66] In the case of the particulate system, however, as was mentioned earlier, hydrodynamic wall effects and electrostatic force field effects play an important role. Modeling of a mechanism is therefore complicated by the need to sort out all of these effects in terms of fundamentally based terms. One approach[32] has been to assume that a large pore system, such as the 2.5-μm Fractosil packing, can be treated as a matrix of interconnected capillary tubes through which solvent and particle flow occur. Separation is therefore purely hydrodynamic since particles are assumed to randomly sample by convection both the flow-through packing pores and the interstitial void spaces during transit through the bed. In such a case one has precisely the conditions for separation assumed in the earlier HDC model for macromolecules.[12,13] Consequently, the derivation for the separation factor for a particle passing through a parallel array of such small and large capillaries follows in analogous fashion.[32] The relevant expression is

$$\frac{1}{R_F} = \frac{f_o}{R_{F,o}} + \frac{f_i}{R_{F,i}} \tag{24}$$

where $f_o$ and $f_i$ are volume fractions of the bed consisting, respectively, of large diameter interstitial flow-through capillaries and small diameter, flow-through pore phase capillaries. The $R_F$ terms refer to the HDC separation factors for each capillary type.

The formalism developed for the HDC separation factor carries over directly to this case, and one obtains expressions of the form given by Equations 5 and 8. Thus for the particle average velocity in a capillary of type j:[32]

$$\langle v_p \rangle_j = \frac{\int_0^{R_{o,j}-R_p} v_p(r) \exp(-\phi/kT)\, r\, dr}{\int_0^{R_{o,j}-R_p} \exp(-\phi/kT)\, r\, dr} \tag{25}$$

where the capillary radius $R_{o,j}$ is given by the hydraulic radius (Equation 21) for the interstices and the actual pore radius for the packing phase. Essentially the same arguments for ionic strength effects, etc. discussed with regard to the HDC model carry over to this case and it is therefore not surprising that calculations for parameter variations show much the same effects as displayed in Figures 9 to 11. Hence universal calibration conditions at low ionic strengths, particle chemistry effects at high ionic strengths, and packing diameter effects occur in essentially the same fashion.[32] For a given set of conditions the calculated $R_F$ values will be greater for the two-phase HDC system since the separation factor associated with the packing pores, $R_{F,i}$ can exert a dominant influence. An interesting feature shown by Figure 18 is that at low ionic strengths the model predicts the possibility of a turnaround in the $R_F$-particle diameter elution behavior reminiscent of the effects found in the high ionic strength region in HDC. In this case, however, the effect is purely hydrodynamic since the low capillary to particle radius ratio causes a domination of the wall effect, γ, over the excluded streamline effect.

A comparison of the model to data is shown in Figure 19 where the only free parameter is $f_o$ (taken as 0.60) since the interstitial pore radius is fixed by assuming a packing diameter of 90 μm. Clearly, the fit is not as good as seen in Figure 11 for the HDC system despite the fact that the Hamaker constant has been adjusted somewhat (0.03 perg).[33] Though the model predicts data trends, the fit is poor, especially in the lower ionic strength region. This may suggest that a partitioning process occurs in this range.

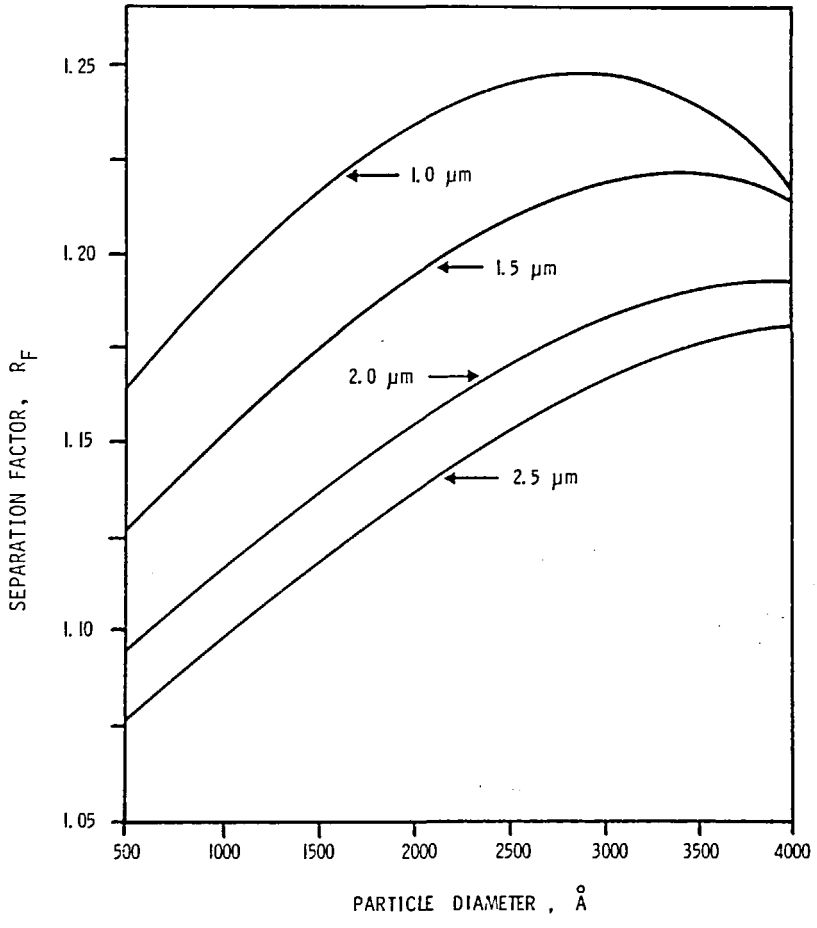


FIGURE 18. Computation based on the porous, flow-through capillary model illustrating the effect of pore diameter on the separation factor at low ionic strength (0.001 *M*). (From Nagy, D. J., Silebi, C. A., and McHugh, A. J., *Polymer Colloids II*, Fitch, R. M., Ed., Plenum Press, New York, 1980, 121. With permission.)

### *b. Pore Partitioning Models*

A recent series of calculations has been carried out aimed at evaluating the separation mechanisms from the basis of a more general chromatography rate theory approach with the objective being to include pore partitioning effects. The formalism is, to a larger extent, built on a combination of the approaches used in the HDC model discussed previously and the ideas inherent in the modeling of size exclusion macromolecular chromatography.[43,63,69] Typically, rate equation analyses for macromolecular SEC have been based on treating the porous matrix as a homogeneous, spherical medium within which radial diffusion of the macromolecular solute takes place,[43,70,71] or, if mobile phase lateral dispersion is considered important, a two-dimensional channel.[72] In either case, however, no treatment of the effects to be expected with charged, Brownian solute particles has been presented from the chromatographic viewpoint.

In order to account for hydrodynamic wall effects and pore partitioning, the bed geometry was assumed to consist of a series of parallel capillaries with attached, cylindrical pores as shown in Figure 20. Essentially the same arguments leading to the area-averaged diffusion equation for an HDC system, Equation 7, were used to obtain the following expression appropriate to Figure 20[67,68] for the particle transport:

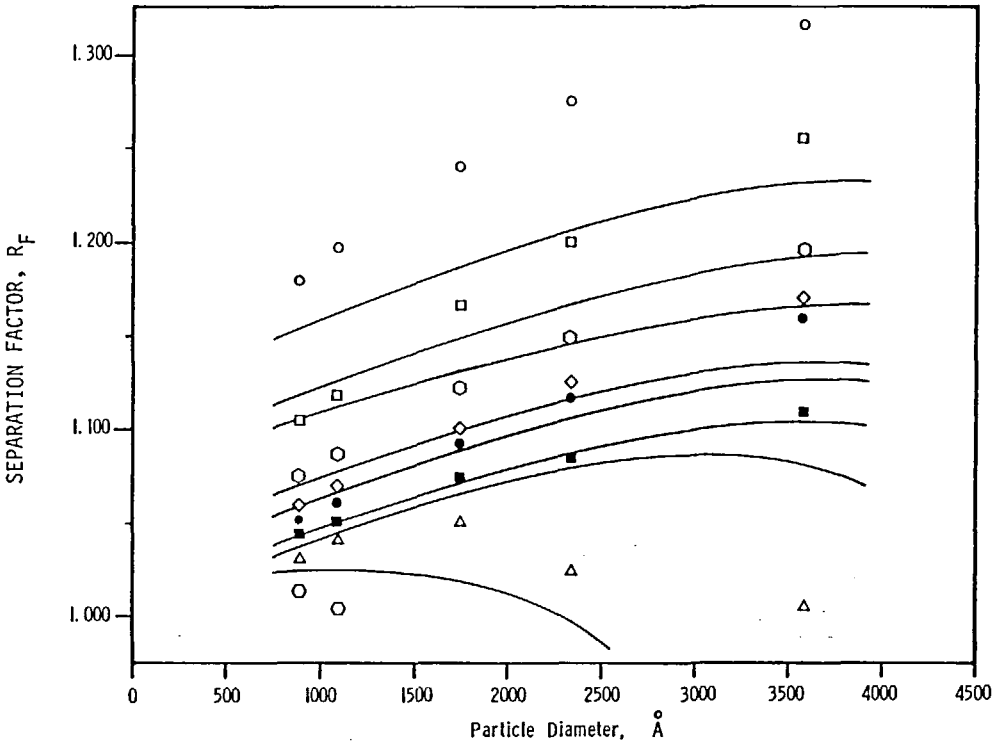


FIGURE 19. Comparison between porous flow-through model separation factor and experimental data of Figure 16. (From Nagy, D. J., Silebi, C. A., and McHugh, A. J., *Polymer Colloids II*, Fitch, R. M., Ed., Plenum Press, New York, 1980, 121. With permission.)



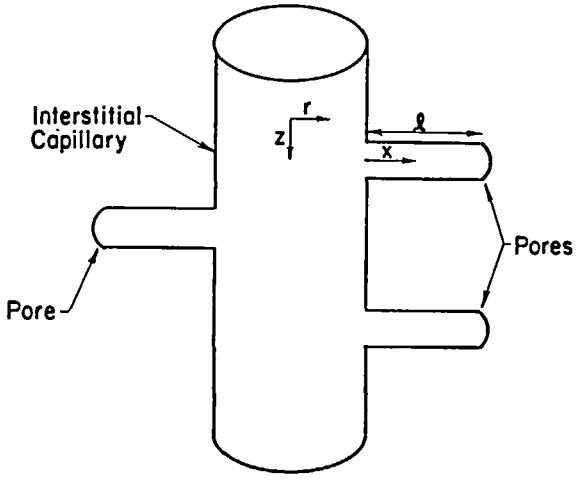


FIGURE 20. Sketch of a capillary-cylindrical pore tube used to model the tube bundle for the porous-partitioning HDC system.[68a]

$$\frac{\partial C_m}{\partial t} + \langle v_p \rangle \frac{\partial C_m}{\partial Z} = \bar{D}^* \frac{\partial^2 C_m}{\partial Z^2} - \frac{(1 - f_o)\bar{D}_s}{\ell f_o} \frac{\partial C_s}{\partial x}\bigg|_{x = 0} \tag{26}$$

All terms in Equation 26 are as defined in Equation 7. The principal change is the addition of a transport term to account for the gain or loss of particles due to exchange between the

mobile and stationary pores. The subscript s refers to the stationary or pore phase and $\bar{D}_s$ refers to the appropriately averaged pore phase diffusivity.[39,67] In addition, for the stationary pore phase, assuming one-dimensional diffusional transfer, one has:

$$\frac{\partial C_s}{\partial t} = \bar{D}_s \frac{\partial^2 C_s}{\partial x^2} \tag{27}$$

Equations 26 and 27 were used together with the appropriate initial and boundary conditions:[43,67]

$$C_s = C_m = 0, \text{ for all Z, and } t = 0 \tag{28a}$$

$$C_m \text{ bounded as } Z \rightarrow \infty \tag{28b}$$

$$\int_0^x [f_o C_m + (1 - f_o) C_s] \, dZ = M' \qquad \bar{D}_s\left(\frac{\partial C_s}{\partial x}\right) \Big|_{x = \ell} = 0 \tag{28c}$$

where M′ is the mass of solute particles injected per unit column area. Further, assuming equilibration at the mobile-stationary phase interface:

$$C_s = K C_m \tag{29}$$

where K is the equilibrium partition coefficient. This gives a set of equations very similar to the rate theory model for macromolecular SEC.[6,43] In the case of a particulate system, the partition coefficient becomes[63,67]

$$K = \frac{2}{R^2} \int_0^{R - R_p} \exp(-\phi/kT) \, r \, dr \tag{30}$$

By neglecting axial dispersion effects, a straightforward analysis by Laplace transform is possible and leads directly to the following expression for the particle mean residence time.[67]

$$\theta_p = \left(1 + \frac{K(1 - f_o)}{f_o}\right) \frac{L}{\langle v_p \rangle_o} \tag{31}$$

where the subscript o refers to the interstitial pore. A similar expression obtains for the marker species. Combination of terms similar to that used in deriving Equation 5 gives the separation factor expression for this model:[67]

$$\frac{1}{R_F} = \frac{1}{R_{F,o}} \left( \frac{1 + K \dfrac{1 - f_o}{f_o}}{1 + K_m \dfrac{1 - f_o}{f_o}} \right) \tag{32}$$

In Equation 32, $K_m$ represents the partition coefficient for the ionic marker species, given by an expression similar to Equation 30. These equations show the asymptotic limit one would expect for pure HDC behavior (i.e., $K = K_m = 0$) as well as explicitly showing the effects of particle and marker partitioning on the separation factor. Using Equations 12 and 17 to 20, a series of parametric calculations showed that precisely the same effects concerning ionic strength and packing diameter as seen in the HDC plots (Figures 9 to 12) again results. However, since there are no flow effects in the stationary phase, the hydrodynamic turnaround seen in Figure 18 does not occur. Figure 21 shows the fit obtained to the data of Figure 16.

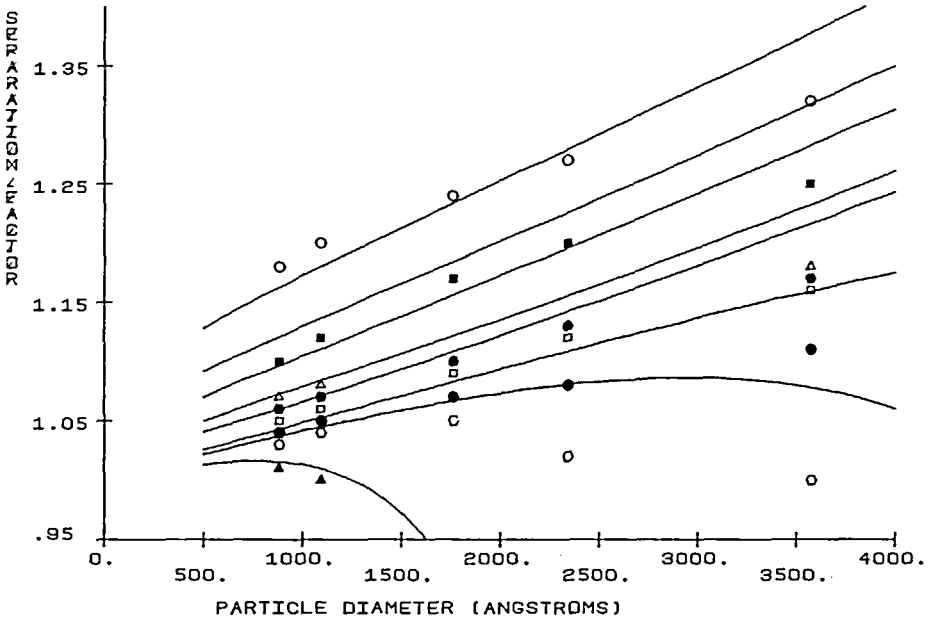


FIGURE 21. Comparison between the data of Figure 16 and predictions of the porous partitioning model.[68a]

The partition model predicts the magnitude of the separation factor better than the parallel capillary model, however, the parallel capillary model predicts the shape of the curves better. This suggests that neither model alone is sufficient to account for the separation.

To investigate the possibility that both porous phase flow-through HDC and partitioning can be contributing to the overall separation, a series of calculations was carried out in which the bed cross section was assumed to consist of a fraction, $f_o$, of parallel large-diameter capillaries to represent the interstitial void volume, a fraction $\Psi$ of which is associated with the geometry of Figure 20. Of the total porous phase volume, $V_i$, a fraction $\psi$ was considered to be stagnant and therefore available for interaction with the particles solely by partitioning. In consequence, the separation factor expression becomes[68a]

$$\frac{1}{R_F} = \frac{f_o}{R_{F,o}} + \frac{(1 - \psi)(1 - f_o)}{R_{F,i}} + \frac{\Psi(1 - f_o)\,K}{R_{F,o}} \tag{33}$$

Equation 33 can be viewed as a general combination to account for all three mechanisms which may occur with a porous system, i.e., HDC in the interstices, HDC in the flow-through portion of the porous phase, and pore partitioning with the stagnant portions of the matrix. Depending on which of these dominates, one obtains the previously discussed limiting forms. For a nonporous system, by definition $f_o = 1$ and Equation 5 results, while for porous systems, two asymptotes are possible. For a purely flow-through system, $\psi = \Psi = 0$ and Equation 24 results, while for a system in which all of the pore volume is stagnant, $\Psi = \psi = 1$ and Equation 32 results for $K_m = 1$. Since at present the model parameters $\Psi$ and $\psi$ are indeterminant, they can only be viewed as arbitrary weighting coefficients to be associated with the two assumed porous phase mechanisms. Nonetheless, as Figure 22 shows, an improved description of the $R_F$ behavior is possible for reasonable values of these parameters.

## C. Conclusions Regarding Separation Modeling

It would appear at this point in its development, that the basic mechanisms involved in packed column particle chromatography are quite amenable to rationalization on the basis

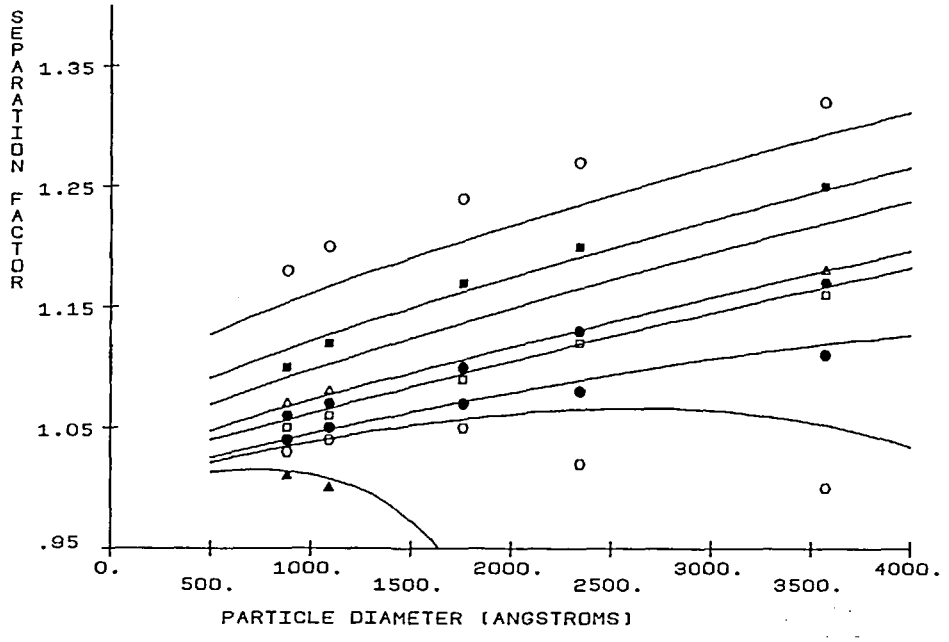


FIGURE 22. Comparison between the data of Figure 16 and predictions of the combined porous flow-through and partitioning model.[68a]

of the HDC mechanism for nonporous systems and some combination of HDC and pore partitioning mechanisms for porous systems. The model fit for nonporous HDC is more satisfying since the $R_F$ behavior can be quite accurately described by a zero-free parameter calculation. Conclusions regarding separation modeling for porous systems are more tentative since three extra parameters ($f_i$, $\psi$, and $\Psi$) have been arbitrarily added and, as yet, no experimental studies specifically addressed to a comparison of the partitioning process in a column geometry and a nonflow geometry (such as have been used to discriminate between separation mechanisms in macromolecular SEC[73-76]) have been reported. Such studies would be useful in determining how best to model the porous packing process and presumably, also, how best to optimize packing properties for a given separation. It is also important to note that the equilibrium partitioning coefficient has been added in an ad hoc fashion to the model equations, and therefore the analysis offers no real insight into the dynamics of the mobile phase-stationary phase transfer process.

All of the models and studies discussed to this point have been concerned with the mean residence time behavior of the particles. A complete theory needs to address the important question of band broadening effects since these can exert a severe influence on the ultimate resolution of a given system. In the next sections, discussion will be directed towards the practical aspects of particle size distribution analysis and column separation resolution. These will be followed by a very brief critique of the attempts which have been made to address band broadening from a fundamental viewpoint.

## III. PARTICLE SIZE DISTRIBUTION ANALYSIS AND COLUMN RESOLUTION

Average particle sizing by column chromatography is a fairly straightforward process, readily adaptable to on-line quality control. By operating under conditions of universal calibration or by making comparisons to calibration data taken under fixed conditions, one can readily convert output chromatogram peaks to "average" particle diameters. The use-

fulness of the HDC method is that one is measuring a response (average residence time) which reflects the *in situ* hydrodynamic behavior of a latex. In consequence, observations regarding, e.g., swellability,[5,10,77] agglomeration effects,[5,10] and particle growth kinetics[5,18] can readily be made. To be discussed shortly, however, one needs to be cognizant that the average size measured depends on the signal response characteristics of the chromatographic detection system and dispersion as well.

The ultimate impact of column chromatography as both an analytical method and tool for experimental studies rests on its ability to give quantitative information on the particle size distribution and not just the average size. Whether one's object is to correct an average diameter or to determine the complete PSD, this means that account needs to be taken of band broadening or axial dispersion effects. With macromolecular SEC, even though separation of peaks corresponding to individual molecular weight species rarely (if ever) occurs, corrections for individual peak overlap often represent minor adjustments to the average MW and MWD.[6] In circumstances where accurate molecular weight distributions are needed, corrections for peak dispersion are necessary. This requires evaluation of the integral equation, due to Tung,[78] which relates the chromatograph signal at elution volume V, F(V), to the corrected chromatogram for the molecular weight species eluting at an average volume, y, W(y):

$$F(V) = \int_0^\infty W(y)\, G(V,y)\, dy \tag{34}$$

The function G(V,y) represents the normalized instrumental spreading function for a given species. Methods for solving Equation 34 have been reviewed elsewhere.[8]

The formalism for converting a particle chromatogram to a size distribution follows the same approach one would use for macromolecular SEC. Thus G(V,y) becomes the normalized particle dispersion function for particles of a given diameter and W(y) represents the area under the chromatogram associated with the particle diameter having an elution volume y. One very critical difference is in relating the detector signal characteristics to particle numbers. In SEC with refractive index difference, the signal is proportional to concentration and generally independent of molecular weight, thus W(y) is usually directly proportional to concentration.[6] For particle suspensions, the signal will in general depend quite strongly upon particle size as well as numbers. Thus, e.g., with turbidity, the number of particles eluting with volume, y, N(y), through a detector cell with path length, x′, is related to W(y) through the extinction cross section, $R_{ext}(y)$.[24]

$$N(y) = \frac{W(y)}{x'\, R_{ext}\,(y)} \tag{35}$$

In HDC the entire spectrum of particle sizes from 30 to 400 nm in diameter is encompassed in about a 3-m$\ell$ elution volume (see, e.g., Figure 3). As a consequence, dispersion causes significant peak overlap, and in combination with the nonlinear signal characteristics necessitates the use of axial dispersion corrections of the chromatogram in order to obtain meaningful size distribution results. Calculations for ratios of known bimodal mixtures based on *a priori* knowledge of the particle sizes present indicated that a numerical technique assuming Gaussian dispersion gave results which compared favorably with electron microscopy counts.[24] Later studies, however, have clearly established that the peak spreading is non-Gaussian and this feature, in conjunction with the highly nonlinear dependence of $R_{ext}(y)$ with particle size in Equation 35, leads to the need for accurate fitting of the chromatogram F(V). In consequence, one finds that direct application of the methods developed for GPC analysis leads either to poor matches between calculated and measured PSDs, ill conditioning of Equation 34 (oscillating solutions, etc.), or both.[79]

A very complete study of dispersion and particle size distribution analysis was carried out by Silebi and McHugh.[30,79] These authors compared modifications of a number of the methods used to solve Equation 34 for GPC analysis to HDC column data taken for two polydisperse latex systems. Results are most conveniently presented in terms of normalized distribution functions. As indicated earlier, under low ionic strength conditions one has universal calibration behavior thus enabling use of data for the well-characterized polystyrene standards. In consequence, the normalized differential particle size distribution, $w(D_p)$, where $D_p$ is particle diameter, is given by:

$$w(D_p) = \frac{W(y)}{S\, D_p \int_0^{\infty} W(y)\, dy} \tag{36}$$

where S is the slope of the log $D_p$ vs. elution volume calibration curve.[30,79]

A number of methods were evaluated for converting Equations 34 to 36 to a PSD. Signal characteristics were calculated using Mie theory for the scattering cross section which was demonstrated to adequately describe the photometer response.[79] In order to obtain accurate results using an assumed form for G(V,y), in conjunction with the techniques of integral analysis, the non-Gaussian nature of the individual particle chromatograms had to be included. The form assumed was chosen to emphasize the fit of the resulting chromatogram in the small particle region:

$$G(V,y) = \exp\left[\frac{-(V - y)^2}{2\sigma^2}\right] \sum_{m=0}^{n'} b_m \left(\frac{V - y}{\sigma}\right)^m \tag{37}$$

In Equation 37, $\sigma$ is the square root of second moment of the specie chromatogram, and four coefficients ($b_0$, $b_4$, $b_8$, and $b_{16}$) were used. The function W(y) was expressed as a polynomial expansion:[78]

$$W(y) = \exp\left[-p^2 (y - y_o)^2\right] \sum_{i=0}^{n} R_i (y - y_o)^i \tag{38}$$

in which p and $y_o$ are, respectively, the recipricals of the chromatogram standard deviation and mean. The coefficients, $R_i$, were determined by minimizing the square of the error between the calculated and experimental polydisperse chromatogram, fit to a Hermite polynomial expansion. Although this technique gives PSDs in reasonable agreement with measured values for broad size distribution systems, it did not do as well for systems with discontinuities in the distribution function.

Of the several numerical methods investigated, the most attractive was found to be one which is a variation of an algorithm developed by Ishige et al.[8] for macromolecular SEC. The method has the advantage that since it is fully numerical the normalized chromatograms of the monodisperse standards can be entered directly, thus eliminating the need for a specific spreading function to characterize them. The algorithm starts with a first estimate of W(y) obtained from the polydisperse chromatogram assuming no axial dispersion. From Equation 34 one obtains a first estimate of the chromatogram, F*(v). The distribution W(y) is then corrected at each integration point depending on the error between computed and measured chromatogram. The modified form used to correct W(y) is[79]

$$W_{i,j+1} = W_{i,j} \prod_{k=-n}^{n} \left(\frac{F_i^*{}_{+k}}{F_{i+k}}\right)^{\alpha} \tag{39}$$

where j refers to the level of iteration; F is the actual chromatogram; and $\alpha$ is a weighting coefficient taken from the actual contributions of the neighboring particle sizes within $\pm 2\sigma$ of a given elution volume, i. The number of symmetric terms about $F_i$ (i.e., n) was chosen

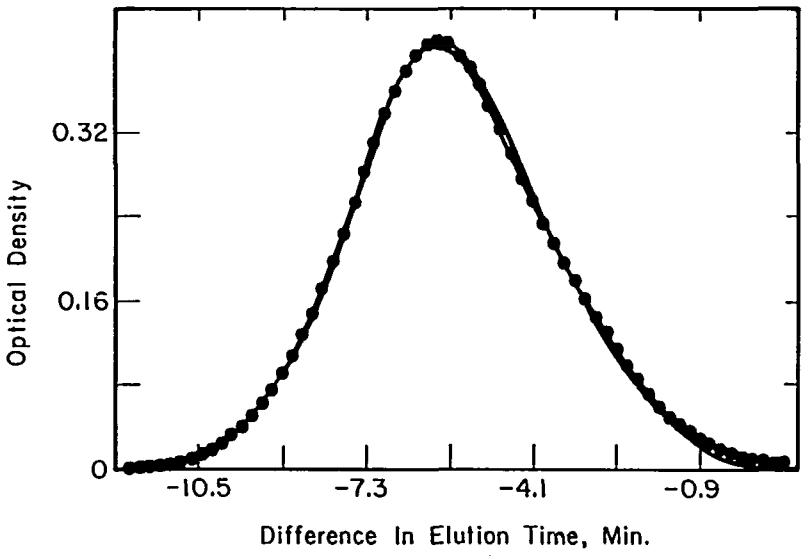


FIGURE 23. Experimental (------) and calculated (—) chromatogram using the modified form of Ishige et al.'s method for a polydisperse polystyrene. (From Silebi, C. A. and McHugh, A. J., *J. Appl. Polym. Sci.*, 23, 1699, 1979. With permission.)



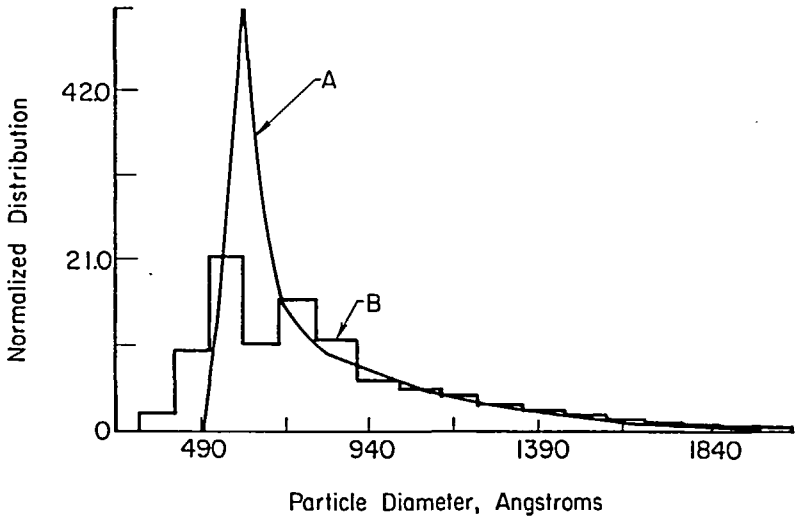


FIGURE 24. Calculated PSD from the chromatogram calculated in Figure 23 (A). Also shown is the PSD histogram obtained from electron microscopy. (From Silebi, C. A. and McHugh, A. J., *J. Appl. Polym. Sci.*, 23, 1699, 1979. With permission.)

to include the $\pm 2\sigma$ spread. Figures 23 and 24 illustrate the chromatogram fit and PSD, respectively, for the polydisperse polystyrene latex. Histogram data for the distribution obtained from electron microscopy are compared to the calculated distributions. These results are typical of the best fits one obtains for distributions which are reasonably broad and contain measurable amounts of small particles. Although the chromatogram fit appears quite

good, one invariably ends up with a relatively poor match between the predicted and measured distribution in the small particle region. This directly reflects the unequal weighting of small particles in the signal conversion relation of Equation 35 in consequence of the sharp drop in the scattering cross section. Thus small mismatches in the measured and calculated chromatogram become magnified. A corollary to this showed up in comparing synthetic chromatograms for various bimodal mixtures of particles where, e.g., a 1:1 by number mixture of 88- and 176-nm particles showed only a small shoulder at the small particle end of the synthesized chromatogram. Nonetheless, the power of the numerical method was demonstrated by resolving the bimodal distribution with a calculated population ratio of 1.5:1.[79]

### A. Resolution Analysis and Improvements

An immediate consequence of the size distribution analysis was the realization that the signal characteristics as well as the dispersion behavior play a dominant role in determining the resolution of a given separation. An instructive approach to this aspect of particle chromatography was taken in a series of papers by Hamielec and co-workers.[64,80,81] Assuming uniform instrument spreading, i.e., G(V,y) = G(V-y), allows analysis of Equation 34 by the Laplace transformation for a convolution integral. Employing a spreading function which corrects the Gaussian shape for skewing[82] in combination with a general expression for the detector response of the form:

$$F(V) \sim N(V)\, D_p(V)^{\Gamma} \tag{40}$$

gave the following expression for the ratio of the corrected, c, to uncorrected, uc, number average diameter from Equation 34:

$$\frac{\bar{D}_p(c)}{\bar{D}_p(uc)} = \frac{1 + \Gamma^3 \alpha' S^3}{1 - (1 - \Gamma)^3 \alpha' S^3} \exp\left(\frac{(2\Gamma - 1) S^2 \sigma^2}{2}\right) \tag{41}$$

In Equation 41, $\alpha'$ is the non-Gaussian correction factor. Thus, in addition to the slope of the calibration curve, S, as mentioned earlier, the magnitude of the correction factor (which is in effect inversely proportional to the resolution) depends upon the non-Gaussian dispersion and on the detector response characteristic, $\Gamma$. One thus finds that for a given column setup, a turbidity detector in the Rayleigh scattering region ($\Gamma = 6$) requires a much larger correction than a refractometer ($\Gamma = 3$). Also, unless one is interested in something like the turbidity-averaged diameter, corrections in general are largest for turbidimetry in the Rayleigh region.

Silebi and McHugh[30,79] carried out a series of calculations which demonstrated that indeed the relative signal intensity of large to small particles for refractive index measurement is superior to that of turbidity in the purely scattering region. In the latter instance a more general form for the refractive index increment based on Mie theory was used so the results could be applied to a wider range of particle sizes. These same authors demonstrated, however, that when one includes the possibility of absorption as well as scattering in the Mie theory calculation for a turbidemetric signal, the improvement in relative signal resolution of small to large particle signals can be dramatic, to the extent of matching and even surpassing that of differential refractometry.[79] An illustration of this important result is given in Figure 25 where the relative weight signals for particles of a given diameter to an equal population of 30-nm particles are shown by the dotted line for a refractometer and the solid lines at different imaginary refractive indices (i.e., amounts of absorption) for turbidity. This observation was felt to be important since experience indicated that the tenfold increase in particle concentration needed for refractometer measurement could lead to column clogging.[30,34,79]

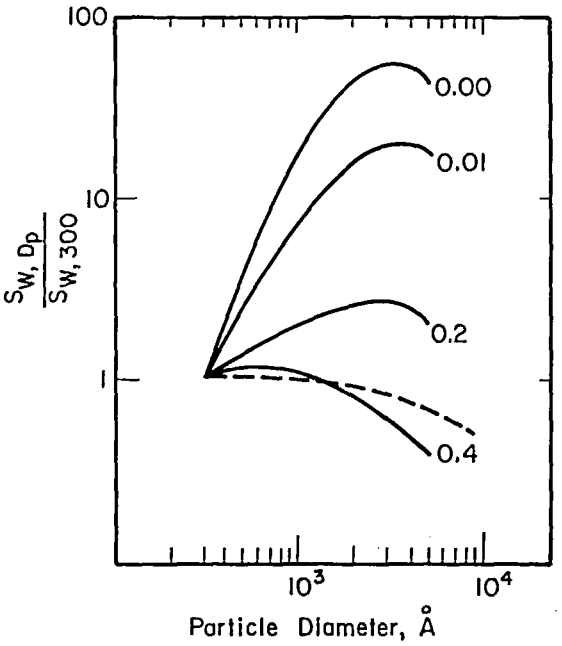


FIGURE 25. Comparison between weight relative signals calculated for differential refractometry (----) and photometric detection at various imaginary refractive index values of colloidal latex particles. Detector wavelengths were 200 nm (photometer) and 500 nm (differential refractometer). (From Silebi, C. A. and McHugh, A. J., *J. Appl. Polym. Sci.*, 23, 1699, 1979. With permission.)



A number of studies have carried out detailed experimental analyses of the effect of the signal resolution characteristics on both HDC and porous HDC systems*.[9,32,61,64,83,84,113] In one series of studies,[9,32,113] corroboration of the superiority of turbidimetric detection in the absorbing wavelength region was established by independent measurement of the scattering characteristics of polystyrene latexes and by HDC chromatogram analysis. Data were reported for the specific extinction coefficient of the Dow polystyrene standards, $k_{ext}$, where

$$k_{ext} = \frac{3}{4\pi} \frac{\rho_{12}}{\rho_2} \frac{R_{ext}}{2.303\ R_p^3} \tag{42}$$

in which the extinction cross section is calculated from the measured turbidity using the Beer-Lambert law; $\rho_{12}$ is the suspension density; and $\rho_2$ is the latex sphere density. Data shown in Figure 26 demonstrate that at a wavelength of 220 nm where the particles begin to absorb, the signal characteristics over the entire particle range show less dramatic changes. The strong dependence of signal intensity with particle size at 254 nm reflects the nature of pure scattering. The difficulty in accurately detecting small numbers of small particles at

* Differences in the light scattering behavior have been reported. Husain et al.[61] observed some discrepancy between calculated and measured extinction coefficients which they attributed to additives in the latices and a size disparity in the particles. As mentioned, such discrepancies were not observed in the study by Silebi and McHugh[79] and other studies from the same laboratory.[9,24,29,32,34,50,62] Experimental values listed in Table I, Reference 61, for the extinction cross section of 109- and 176-nm polystyrene latexes at 254 nm, and attributed to Reference 79, were incorrectly reported. Values of $7.2 \times 10^{-11}$ and $1.89 \times 10^{-10}$ cm² were in fact $5.18 \times 10^{-11}$ and $3.58 \times 10^{-10}$ cm², respectively,[50,79] and these in both cases were less than 30% different than the independently calculated Mie theory values.[29,50] A recent paper,[108] on the other hand, has shown that a good fit between Mie theory and the measurements by Silebi[50] results, assuming adsorption and using an imaginary refractive index of 0.69. These differences have, as yet, not been resolved.

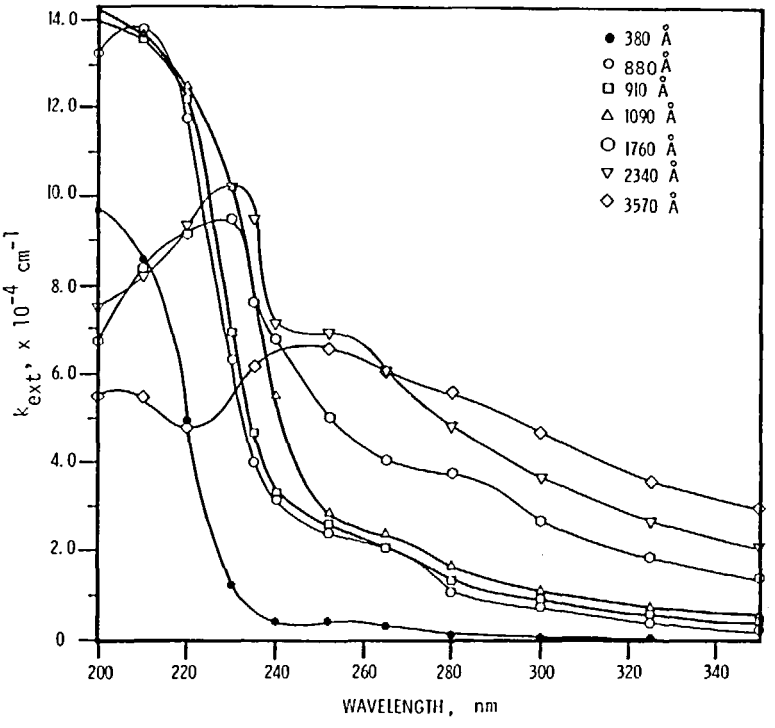


FIGURE 26. Experimental dependence of the specific extinction coefficient for polystyrene latexes of various particle diameter. (From Nagy, D. J., Silebi, C. A., and McHugh, A. J., *J. Appl. Polym. Sci.*, 26, 1567, 1981. With permission.)

this wavelength is indicated, e.g., by the ratio of $k_{ext}$ values for the 234- and 38-nm particles of approximately 16. While at 220 nm, the same ratio becomes 1.8. This effect is dramatically demonstrated in Figure 27 which shows HDC chromatograms obtained using the device described earlier[24] for bimodal mixtures of 38- and 176-nm particles. The small shoulder at 254 nm corresponding to the smaller particle population becomes a well-defined peak at 220 nm, clearly indicating the effects of improved signal resolution. Similar conclusions were evidenced by comparing measured and calculated distributions for a polydisperse latex at the same two wavelengths.[9,62] The conclusion drawn was that for broad size distributions a wavelength for optimal resolution of a given column system will exist.

In the studies of Hamielec and co-workers,[61,64,80,81,83,84] a good deal of attention has been given to the factors affecting the resolution in column chromatography. These are, as already indicated, signal characteristics, peak spreading or axial dispersion, and calibration characteristics. The treatment leading to Equations 40 and 41 can be expanded to include more general scattering behavior, via Mie theory, as well as nonlinearities in the calibration curve. The particle size frequency distribution can be expressed in a form similar to Equation 36 as[61,64]

$$f(V,D_p)\, d\, D_p = \frac{-N(V,y)\, dy}{\int_0^x N(V,y)\, dy} \tag{43}$$

where the minus sign has been introduced to account for the negative slope, S, of the calibration curve. Combining Equations 34, 35, and 43 with the definition of the extinction efficiency factor,[85] $Q = R_{ext}/\pi R_p^2$, gives:

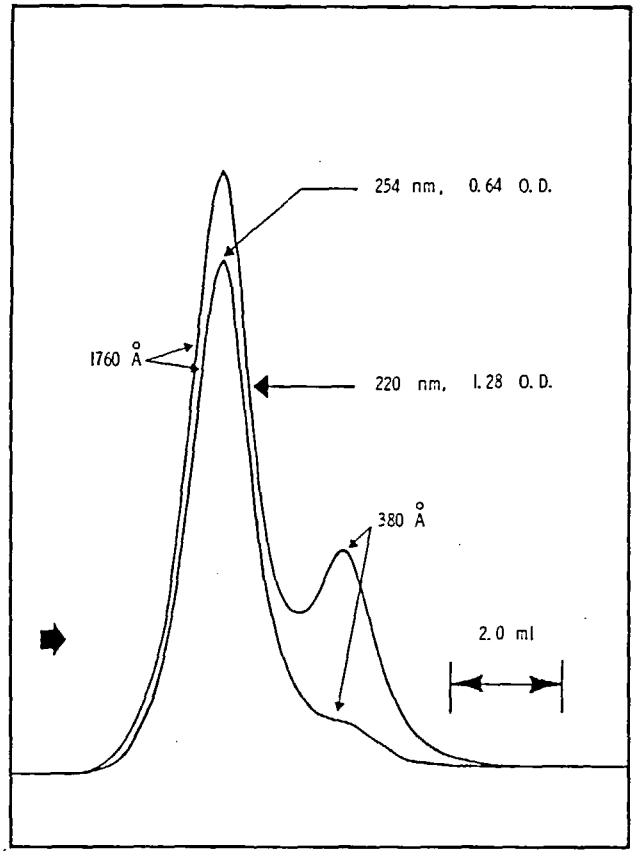


FIGURE 27. HDC separation of a synthetic bimodal mixture of 38- and 176-nm polystyrene monodisperse latexes at 220- and 254-nm detector turbidimetric wavelengths. Weight ratio of the two particle populations is 1.00/1.20. (From Nagy, D. J., Silebi, C. A., and McHugh, A. J., *J. Appl. Polym. Sci.*, 26, 1567, 1981. With permission.)

$$f(V,D_p)\, d\, D_p = \frac{-W(y)\, G(V,y)\, [Q(y)\, D_p^2\, (y)]^{-1}\, dy}{\int_0^{*} W(y)\, G(V,y)\, [Q(y)\, D_p^2\, (y)]^{-1}\, dy} \tag{44}$$

In this form, the dependence of the calculated distribution function on the scattering cross section is made more apparent. Calculations were carried out for diameter averages including all of the effects mentioned and comparisons were made with data on their size exclusion system.[18,61,64] Tabular forms for the various correction factors (of which Equation 41 is, e.g., the result applicable to Rayleigh scattering) enabled ready comparison to the chromatographic results. In line with the earlier discussed study,[79] axial dispersion corrections were found to be significant. One therefore needs to approach average diameters obtained from calibration curve data with some caution.

An analysis of particle diameter averages obtained with a porous LEC system and turbidimetric detection at 254 nm has been carried out by Johnston et al.[60] Their results indicated that skewness in the individual chromatograms can alter the expected sequence of the magnitudes of the various diameter averages and thus needs to be included in the analytical treatment. In another experimental study[28] it was shown that the calibration curve becomes nonlinear in the region $D_p \leq 50$ nm for an HDC system. In consequence of the aforementioned sensitivity of the signal response characteristics in the small particle size range, and the

**Table 7**
**RESOLUTION: HDC VS. FRACTOSIL[62]**

| | $R_s$ | | |
|---|---|---|---|
| | HDC | | Fractosil |
| Particle populations (Å) | Three columns | One column | One column |
| 880/1760 | 0.62 | 0.41 | 0.14 |
| 880/2340 | 0.91 | 0.61 | 0.24 |
| 880/3570 | 1.45 | 0.94 | 0.41 |
| 1090/2340 | 0.71 | 0.49 | 0.23 |
| 380/880 | 0.33 | 0.23 | 0.11 |
| 380/1090 | 0.51 | 0.36 | 0.12 |
| 380/1760 | 0.95 | 0.64 | 0.26 |
| 380/2340 | 1.23 | 0.83 | 0.36 |
| 380/3570 | 1.78 | 1.17 | 0.54 |
| | W | | |
| | HDC* | | Fractosil |
| $D_p$ (Å) | Three columns | One column | One Column |
| marker | 1.93 | 1.06 | 8.45 |
| 380 | 2.48 | 1.16 | 12.03 |
| 880 | 2.36 | 1.13 | 12.85 |
| 1090 | 2.36 | 1.07 | 12.67 |
| 1760 | 2.16 | 1.07 | 12.34 |
| 2340 | 2.12 | 1.04 | 11.85 |
| 3570 | 1.88 | 1.02 | 11.75 |

$W = 4\sigma$, the width of the chromatographic peak at the baseline (m$\ell$).



nonlinearity of the calibration curve, an increased sensitivity of the calculated and measured PSDs was found.[34] These studies offer quantitative illustration of the importance of signal, dispersion, and calibration corrections for both average sizing and PSD analysis particularly when broad distributions with measurable numbers of small particles are being analyzed.

Instructive comparisons of relative column performance can often be made by looking at the simpler measures of resolution used in chromatography theory, such as the number of theoretical plates and the column resolution factor.[6] The efficiency of a given system is generally typified by the number of theoretical plates, $16\ V_R^2/W^2$, associated with the marker, where W is the peak base width and $V_R$ is the elution volume. Typically, one finds that the HDC systems exhibit theoretical plate counts in the range of several thousand per foot,[5,62] while the porous systems are in the range of several hundred.[60,62] Comparisons of the specific resolution factors, $R_s$, enable a more precise analysis since both the separation factor and peak dispersion are included. A simple form for the specific resolution between two particle populations is[62]

$$R_s = \frac{\ell n\ (D_{p_2}/D_{p_1})}{S\ W_a} \tag{45}$$

where $W_a$ is the arithmetic average of the elution volume peaks associated with any two particle populations. One finds that although the slope of the calibration curves for porous systems is generally less than that of HDC systems, axial dispersion in the former is con-

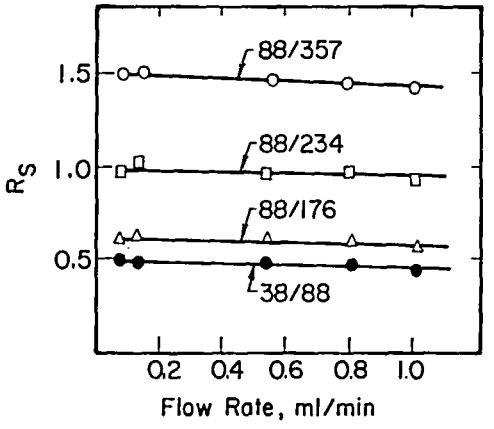


FIGURE 28. Effect of flow rate on specific resolution in an HDC system for various particle sizes in nanometers. (From Silebi, C. A. and Viola, J. P., *Org. Coat. Plast. Chem.*, 42, 151, 1980. With permission.)



siderably greater, resulting in poorer overall resolution. Table 7 shows the data from Reference 62 which demonstrates this effect. A dramatic demonstration of the reduced resolving power of the Fractosil system as compared to an HDC system was shown by comparing predicted and measured distributions for a bimodal latex chromatographed through both.[9] The HDC showed good resolution (both measured and calculated) of both populations, while the Fractosil system was unable to resolve the presence of the two species.

An important observation regarding the resolving power of an HDC system was carried out by Silebi and Viola[86] using the system previously described.[24] Figure 28 shows their experimental results for the HDC column resolution for several pairs of the monodisperse polystyrene samples as a function of the eluant flow rate. These results show that the resolution is independent of flow rate and therefore the time of analysis of a sample can be significantly reduced without substantially affecting the resolution.[86] This observation demonstrates a critical feature of high performance operation.

The high performance potential of HDC has in fact recently been demonstrated.[27] The principal objectives of the study were to show that reduced residence times were possible without loss of resolution and to illustrate a user-based algorithm approach to the data analyses. A cation exchange resin having a nominal diameter of 15 μm was used as packing in a 10 mm-i.d. stainless-steel column. Non-Gaussian dispersion behavior in the calibration standards was fit to a numerical algorithm based on the Pearson type VII model.[27] The detector turbidity response at 254 nm was generated experimentally and fit to two separate polynomial forms. Optimization of signal resolution by using different wavelengths was not considered to be a factor since the study was primarily aimed at particle sizes in the range greater than 100 nm. The algorithm used to compute PSDs was similar in form to that of Ishige et al. discussed earlier with regard to Reference 79. A key feature is that using a somewhat smaller packing diameter and much higher flow rates (~2 vs. 0.6 mℓ/min), the analysis time could be reduced from 90 to 120 down to 5 to 10 min.

### B. Modeling Axial Dispersion Mechanisms

The discussions to this point largely have emphasized dispersion and size resolution from the viewpoint of corrections to the size distribution calculation. One of the important features regarding the advances made in high performance SEC has been that a reasonably mature theoretical structure has developed, in hand with the experiments, to aid in understanding and optimizing the conditions for minimizing axial dispersion. Unfortunately, a similar set

of circumstances with particle chromatography has yet to emerge. Sophisticated analyses of particle dispersion in flow-through porous media have been developed and the area is quite active.[44-46] However, in consequence of the added complications of wall effect and potential field effects, discussed earlier, the transport equations for colloidal particles become less amenable to simple analysis. Since the general subject of particle dispersion behavior is still relatively new, few direct applications to particle chromatography have been attempted. A brief discussion of several aspects of the published works on particle dispersion in chromatographic geometries will be given here. For more detailed general discussions of particle dispersion, References 44 to 46 are recommended.

In their HDC model, DiMarzio and Guttman[12] developed expressions for the axial dispersion to be expected during flow through the interstitial, cylindrical capillaries. Their result for the peak variance, $\sigma'$ (in units of length), can be expressed as

$$\sigma' = (2\, K_d\, \theta_p)^{1/2} \tag{46}$$

where $K_d$ is the modified Taylor-Aris dispersion coefficient given for the particle in terms of the constant diffusivity D by:

$$K_d = D + \frac{v_o^2 R_o^2}{192\, D}\left(1 - \frac{R_p}{R_o}\right)^6 \tag{47}$$

In this expression the particle diffusivity, D, is given by the familiar Stokes-Einstein relation.[54] As pointed out by Brenner and Gaydos,[39] the analysis leading to Equations 46 and 47 does not properly account for the hydrodynamic wall effect nor does it incorporate force field effects. Nonetheless, it has been applied to data on an HDC system.[24] A shortcoming of the model is made apparent by considering the particle size dependence predicted by Equation 46. Since the convection term normally dominates, the leading term in Equation 47 can be neglected. Using Equation 10 for the particle species and noting that in the DiMarzio and Guttman treatment $\gamma = \phi = 0$, one obtains from Equations 8 and 11 the following expression for $\theta_p$:

$$\theta_p = \frac{L}{v_o\left[1 - \frac{1}{2}\left(1 - \frac{R_p}{R_o}\right)^2\right]} \tag{48a}$$

Combination of this result with Equations 46 and 47, along with the Stokes-Einstein relation for $D(kT/6\pi\eta R_p)$, gives

$$\sigma' = \sqrt{\frac{\pi\eta v_o L R_o^3}{16kT}}\left(\frac{(R_p/R_o)\,(1 - R_p/R_o)^6}{1 - \frac{1}{2}(1 - R_p/R_o)^2}\right)^{1/2} \tag{48b}$$

when $\eta$ is the eluant viscosity. Equation 48b predicts that peak dispersion will increase with particle radius (i.e., the decreased diffusivity counterbalances the "excluded volume" effect) up to a particle-to-tube radius ratio of about 0.1. Since $R_o \sim 3$ μm, this corresponds to a particle diameter of ~600 nm. This predicted trend is in direct opposition to experimental observations[27,29,34,62] which show that peak spreading in HDC decreases with increasing particle size. Thus the use of Equations 46 and 47 appears unwarranted.

An apparent shortcoming to the parallel tube model is that, though it offers an excellent vehicle for predicting particle mean residence time behavior, it does not adequately describe stream splitting and other random mixing effects. Silebi and Viola[86] have looked at the capillary network model developed by Saffman[112] in which macroscopic mixing effects are

accounted for by using a statistically isotropic network of capillaries. Modifying the analysis of Saffman, in the fashion of DiMarzio and Guttman they obtained the following expression for the dispersion coefficient:

$$\frac{K_d}{D} = \frac{1}{3} + \frac{3}{80} Pe^2\left(1 - \frac{R_p}{R_o}\right)^6 + \left(\frac{\ell'}{R_o}\right)^2 \frac{Pe^2}{4} \int_0^1 (3\mu^2 - 1)\frac{McothM - 1}{D_1 M^2} d\mu \quad (49)$$

where

$$M = \frac{3}{2}\frac{Pe}{D}\left(\frac{\ell'}{R_o}\right) \text{ and } D_1 = 1 + \frac{3}{16} Pe^2\mu^2 \left(1 - \frac{R_p}{R_o}\right)^6 \quad (50)$$

In Equations 49 and 50 the Peclet number is given by $Pe = qR_o/D\epsilon_v A_c$; $\ell'$ is the capillary length; and $\mu$ is the cosine of the angle between the net direction of flow and the orientation of the capillary tube. However a shortcoming similar to that of the DiMarzio-Guttman model still holds in that Equations 49 and 50 predict the same increasing trend of $K_d$ with particle size. This can readily be confirmed by numerical computation or by applying limiting arguments similar to those employed to derive Equations 46. It is interesting that a good fit between the model calculations and experiment resulted.

With porous particle chromatography, trends in the dispersion behavior have not been as well defined as HDC. In some studies peak spreading has been observed to increase with particle size to some intermediate value and then decrease,[60,62] while in others a monotonic decrease in spreading with increasing particle size has been reported,[18,64] or a variation in pattern,[61] all depending upon the particulars of the packing-column geometry and eluant ionic strength employed. Clearly a number of effects are being superimposed on the process, not the least of which is the pore partitioning. In the latter instance, the simplified analysis by McHugh and Francis[68] discussed earlier, leads to the following expression for the chromatogram second moment, $\mu_2$:

$$\mu_2 = \frac{2}{3}\left(\frac{K\,\ell^2\,f_o}{(1 - f_o)\,\bar{D}_s}\right)\frac{L}{\langle v_p \rangle} \quad (51)$$

where $\ell$ is the partition capillary length as shown in Figure 20. This expression represents the contribution of peak spreading associated with the partitioning process. As yet, however, no controlled experimental analyses have been carried out to find conditions under which limiting forms of the dispersion might occur. Such studies are much needed since they could provide valuable insights into controlling mechanisms.

As pointed out earlier, dispersion in porous bed flows of molecular solute species has been successfully treated in terms of the pseudocontinuum models which incorporate dispersion coefficients as parameters to be determined experimentally. Such an approach has proved useful in evaluating axial dispersion in LEC.[87] Brenner[44] has pointed out that many of the major global features of the dispersion behavior of particles, including wall and potential field effects, can be treated by a formalism similar in philosophy to that of the Taylor-Aris theory. The formalism of this approach has been used to some extent in a simplified form in this review in the discussion of separation mechanism modeling of HDC and porous particle chromatography. Further work along these lines should prove useful in the development of fundamentally based descriptions of dispersion in particle chromatography.

### C. Further Applications of Packed Column Methods

From the early studies reporting fractionation of viruses using porous glass[88] and proteins using nonporous glass,[11] to the present day applications of particle chromatography, it is becoming clear that distinctions between macromolecular and colloidal separation processes

may be more a question of whether the solute behaves as a flexible coil or a hard particle, rather than one of dimensions. Attesting to this are the studies of colloidal suspensions[17,18,59,89] and micellar suspensions[90] in porous systems wherein the particles are well within the range of macromolecular coil size. Several recent studies indicate that HDC may in fact have considerable promise as a method for the analysis of ultrahigh molecular weight macromolecules.[91-94] In such cases, application of conventional SEC techniques has frequently yielded little, if any, information about molecular weight or molecular weight distribution.[95,96] Studies with xanthan polysaccharide, partially hydrolyzed polyacrylamides, and dextran[93] were carried out since these represent the full spectrum of polymer conformations: rigid rod, flexible linear chain coil, and flexible branched chain coil, respectively. In one study[94] molecular weight distribution data for a xanthan system were obtained. By using the polystyrene latex calibration curve, $R_F$ values for the macromolecules were converted to effective spherical sizes. Analysis of the separation factor mechanism in terms of hydrodynamic models for the rigid rod systems is complicated by the need to analyze the effect of flow on the rod average orientation,[92] and macromolecular migration due to the spatial variation of the velocity gradient.[94] In the former instance one finds the rod orientation, hence separation factor will vary with flow (i.e., shear rate), and predictions are sensitive to whether one assumes elongational or shearing flow in the interstices.[92]

By way of summary, it is apparent that packed column, particle chromatography is a powerful tool for the analysis of colloidal particulate suspensions particularly in the submicron range. In some circumstances (dispersion analysis in particular) the practical methods which have been developed for optimizing resolution are in need of a fundamental theoretical explanation in order to truly optimize the design of a given system. It appears, at this point, that the separation mechanism for HDC is well described by the capillary bed model, but for porous systems more work is needed to determine which of the possible mechanisms controls the optimal separation.



## IV. CAPILLARY HYDRODYNAMIC CHROMATOGRAPHY

The use of narrow bore capillary tubes for chromatographic analysis of particulate suspensions has many features in common with HDC and in some sense, particularly with submicron-sized particles, might be viewed as a variation on the process. As pointed out in the introductory section, however, since one is generally dealing with much larger particle size ranges, the operative hydrodynamic mechanisms can, at least in theory, vary from that of Browman motion-driven preferential sampling of fluid streamlines (i.e., the HDC mechanism) to a completely hydrodynamically driven lateral migration (i.e., the tubular pinch effect[97]). The method appears most applicable to particles larger in size than 1 μm, under which conditions the operable mechanism is most likely tubular pinch. However, it should be pointed out that separations at the macromolecular scale have also been reported with this method.[98] Experimental setups for capillary chromatography are essentially the same as the packed column systems except that the column itself consists in this case of coiled stainless-steel tubing having an inside diameter on the order of 254 μm and lengths on the order of several hundred feet.[19,20,99] Signal measurement, calibration techniques, and average particle sizing are very much the same as in HDC. There have been relatively few published studies of the method, however, sufficient work has been done to justify several general observations and comparisons to the packed column methods.

A very complete study was carried out by Noel and co-workers[20] investigating the sizing characteristics of a system comprised of 200 ft of 0.015-in. I.D. tubing, a standard injection valve, and an absorbance monitor. A range of particle systems was investigated including polystyrene latex standards, pollen, bacterial spores, silica, and whole cells. In the case of latex suspensions, addition of ethylene glycol to the eluant phase was necessary to avoid

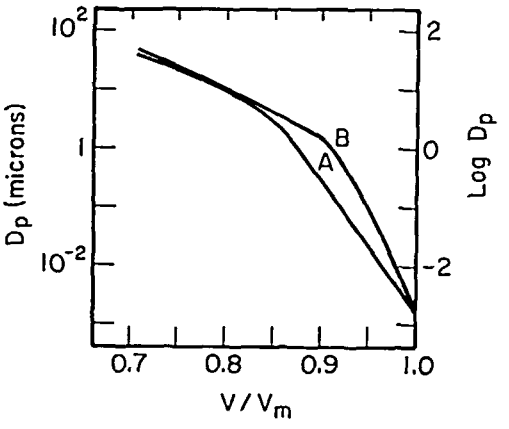


FIGURE 29. The effect of column diameter on the capillary chromatography calibration curve. Column A is 300 ft × 0.015 in. I.D. Column B is 500 ft × 0.02 in. I.D. Mobile phase, 1% ethylene glycol in water. (From Noel, R. J., Gooding, K. M., Regnier, F. E., Ball, D. M., Orr, C., and Mullins, M. E., *J. Chromatogr.*, 166, 373, 1978. With permission.)



aggregation. Typical mobile phase flow rates were on the order of 1 to 2 mℓ/min; thus, mean residence times were typically several minutes. A schematic illustration of the separation factor (calibration curve) behavior observed in this study is shown in Figure 29. Two features are apparent, the first being that two separation regions of behavior are clearly observed with the break-off point occurring around a particle diameter of 1 μm, and second, resolution is much higher in the larger particle region since resolution of peak separation is again inversely proportional to the slope. Unlike the behavior seen in the packed column systems, the $R_F$ factor is not constant with flow rate. This makes it apparent that size determinations of unknowns must be carried out at the same flow rate used to develop the calibration curve.[20]

Another very important feature of capillary chromatography is the effect of flow rate on the specific column efficiency as shown by the plate height behavior illustrated in Figure 30 for a 10-μm silica particle and a molecular marker species, glycyl-L-tyrosine. Plate heights are considerably larger than packed column HDC (the latter being on the order of 0.1 mm[5,62]), and for solute size particles, increases in height with flow rate occur, while the reverse results for the larger particles. This clearly indicates that the two mechanisms operable in capillary chromatography represent dramatically different dispersion behavior and in the case of the large particles a minimum velocity is needed to "focus" the particles.[20] It was also observed that increasing column length increased the plate height, eventually destroying the resolution. A further important observation was that the separation mechanism for small particles is dependent on viscosity, while that for large particles is viscosity independent.[20]

Studies by Mullins and Orr[19] and Poehlein,[99] on similar systems, reported results virtually identical to those of Noel et al. Brough and co-workers[110] extended the useful fractionation range for capillary HDC by further studying the effects of tube diameter, eluant viscosity, and flow rate. Three capillary columns of equal length (50 m) but different internal diameter (152, 203, and 254 μm) were studied using various particle standards in water, methanol, or tetrahydrofuran (THF). Consistent with the results found by Noel et al., an increase in column resolution was observed with increasing flow rate. Their results also indicated that electrical interactions between the particles or particles and capillary wall were of little consequence.

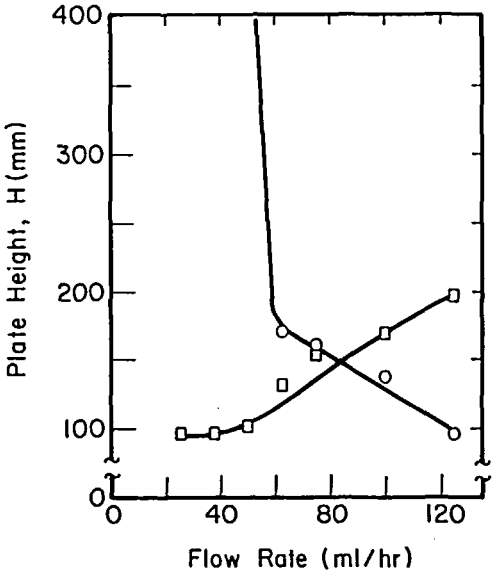


FIGURE 30. Effect of flow rate on plate height in capillary chromatography for a 10-μm silica particle (○) and glycyl-L-tyrosine (□). (From Noel, R. J., Gooding, K. M., Regnier, F. E., Ball, D. M., Orr, C., and Mullins, M. E., *J. Chromatogr.*, 166, 373, 1978. With permission.)



## A. Separation Mechanisms in Capillary HDC

Although only qualitative discussions of the separation mechanisms operable in capillary HDC have been given, it is clear from the data that the most probable explanation is that tubular pinch is occurring for the particles above 1 μm and an HDC mechanism is occurring below.[19,20] The tubular pinch or radial migration phenomenon has been attributed to nonlinear inertial effects[35,100,114,115] which cause a particle injected into a Poiseuille profile to preferentially migrate away from the tube axis and tube wall, reaching an equilibrium at some eccentric position. A complete analytical description of the phenomenon has not to date been available, thus, an extensive discussion would be premature and trends consistent with this mechanism can only be viewed semiquantitatively. Certainly in all cases, tube Reynolds numbers are such that one is dealing with Poiseuille flow. Using the criterion given by Brenner (Equation 2.62 of Reference 35), one also finds that the particles are clearly neutrally buoyant. Thus analysis in terms of the tubular pinch effect is appropriate. In such a case the particle Reynolds number $Re_p$ based on the slip velocity has been used to correlate the onset of particle migration.[100] From the definition of $Re_p$, one obtains from Equation 11:

$$Re_p = \frac{4R_p V_o \left(\frac{R_p}{R_o}\right)^2}{3\nu} \tag{52}$$

where $\nu$ is the kinematic viscosity and the value of 2/3 is used for $\gamma$. It seems reasonable to relate the minimum velocity effect in Figure 30 to the particle Reynolds number needed for appreciable lateral migration (i.e., $Re_p > 10^{-3}$ [35,100,101]). For the data of Figure 30 one finds a value of $Re_p > 2.6 \times 10^{-2}$ which may be close enough to warrant the qualitative explanation given on this basis.[20] Likewise, the effect of decreasing particle residence time

with increasing size and eluant velocity[19,20] is fully in line with the tubular pinch effect,[100,101] as is the reduction in dispersion.

At the other end of the spectrum, for the particles less than 1 μm in diameter, one is tempted to associate the $R_F$ behavior with the HDC effects analytically described by the model discussed earlier, since significant Brownian motion begins to occur in this size range. The observation of peak spreading increasing with flow (see Figure 30) would also be at least qualitatively consistent with Brownian solute dispersion behavior as described, e.g., in Equation 47. On the other hand, the axial distance the particle must travel before Brownian diffusion has enabled at least one sampling of the transverse radial profile can be estimated from the argument given by DiMarzio and Guttman.[12] Neglecting wall and potential field effects, one finds the required tube length, $L_{req}$, to be given by:

$$L_{req} = \frac{3\pi\eta R_o^2 <v> R_p}{kT} \tag{53}$$

Substitution of typical values shows that in order to achieve a steady state, one would need tube lengths at least one to two orders of magnitude greater than those used. It may well be that an explanation for the flow rate, tube diameter, and viscosity dependence of $R_F$ is a reflection of a transient, Reynolds number-dependent, Brownian transport process. However, more detailed experimental analyses would be needed before the limits of either mechanism can be mapped precisely.

Because of its simplicity, ease of operation, and ability to handle a wide range of particle sizes and types (as well as a range of eluant conditions[110]), capillary chromatography appears to be an attractive technique for average particle sizing. In its current state, it is most suited for large particles, where the mechanism of separation, though not quantitatively described, is well behaved and predictable on the basis of the tubular pinch effect. However, use of the method for size distribution analysis has yet to be demonstrated and its application to submicron sizing is presently less efficient than HDC.



## V. FIELD-FLOW FRACTIONATION

As indicated in the introduction, field-flow fractionation (FFF) refers to a general class of techniques which, like HDC, can be thought of as one-phase chromatography since solute retention is a consequence of applied forces as opposed to a partitioning between phases. The forces used for this purpose are thermal gradients, sedimentation forces, electrical forces, or lateral flow displacements.[22] In some sense, the fundamental distinctions between HDC, TPC, and FFF become blurred in that, in each case, the convected transport of the solute particles is being influenced by interaction with a force field. The principal distinction is an operational one (and is indeed quite important) in that HDC and TPC involve solely internally generated force fields (electrostatic or hydrodynamic), while in FFF an externally controlled field is being applied in a programmed fashion to affect the residence time of a given species. Interesting and complete discussions of the classification of separation methods in general,[40] and size separation in particular,[102,103] are available elsewhere and are recommended to the interested reader.

The development of FFF methods has been pioneered by Giddings and co-workers and a voluminous literature has evolved on the subject. The methods have been applied to macromolecular and particulate systems with varying degrees of success. Since excellent reviews are available on the general subject,[22,104] this section will not be intended as one. Attention here will instead be directed to a brief review of one of the most recent developments in this area, that of sedimentation FFF (SFFF), since it appears to offer great promise as a particle size analysis tool. The technique, to some extent, has features in common with that of the high speed disc-ultracentrifuge,[3] however, the method of operation is different and the resultant resolution appears superior.

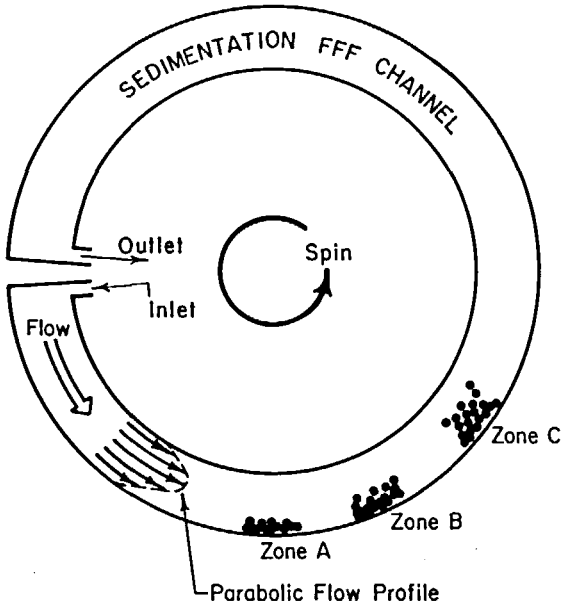


FIGURE 31. Side view of sedimentation FFF channel in a centrifuge. Zones A, B, and C represent particles of different size (A largest and C smallest). (From Giddings, J. C., Karaiskakis, G., Caldwell, K. D., and Myers, M. N., *J. Colloidal Interface Sci.*, 92, 66, 1983. With permission.)



An excellent description of the experimental operating characteristics is given in References 105 and 106. Figure 31 shows a side view of the SFFF device which consists of an open channel formed between two closely spaced parallel surfaces. Eluant is pumped through the channel, and upon injection of particles, the carrier flow is interrupted while the entire device is rotated in a centrifuge. This causes larger particles to concentrate closer to the wall where the fluid streamline velocities are least upon return of the flow. In consequence of this continuous interaction between field and flow, smaller particles will elute first followed by particles of increasing mass (just the reverse of the column methods). Signal measurement by light scattering, refractive index increment, viscosity, etc. is carried out at the channel exit and one develops thereby a chromatogram.

Equation 6 again governs the convective-diffusive behavior of the solute particles. During the rotation cycle a steady gradient develops in the x direction which in this case is taken to be the coordinate dimension normal to the wall of Figure 31 at which the solute accumulates. Setting the flux term in Equation 6 equal to zero then allows calculation of the concentration profile $c/c_o$ over the column width:

$$\frac{c}{c_o} = \exp \frac{-x}{\ell_c} \tag{54}$$

in which $\ell_c$ is a length parameter which characterizes the solute layer thickness.[106] In deriving Equation 54, the expression for the drift velocity induced by centrifugation was employed in which wall effects were neglected.[106] The potential field term, $\nabla\phi$, in Equation 6 was also neglected. The solute, concentration-averaged velocity during flow can then be calculated using Equation 54 and from this the separation factor. It should be noted that the mode of solution is in essence the same approach used to derive the HDC separation factor, except in the latter case the radial "drift" velocity arises solely from the potential field term. The derivation associated with Equations 7 and 54 in this paper and that used in

Reference 37 point out that the fundamental similarities of these analyses arise from the fact that they are based on the same transport equation (i.e., Equation 6).

For monodisperse particle populations, the following relationships hold for the separation factor:[106]

$$R_F = 6\lambda'[\coth(1/2\lambda') - 2\lambda'] \tag{55a}$$

where $\lambda'$ is the dimensionless retention parameter:

$$\lambda' = \frac{\ell_c}{w_c} \tag{55b}$$

in which $w_c$ is the column width. For spherical particles of diameter $D_p$, $\lambda'$ is related to the centrifugal acceleration, $G_c$, and the density difference between the particle and eluant, $\Delta\rho$, by:

$$D_p = \left(\frac{6kT}{\pi G_c w_c \lambda' \Delta \rho}\right)^{1/3} \tag{56}$$

For large particles, Equation 55a needs to include a steric correction factor,[107] otherwise upon combination of the limiting form for $\lambda \rightarrow 0$, one obtains the simple relation:

$$D_p = \left(\frac{36kT}{\pi G_c w_c R_F \Delta \rho}\right)^{1/3} \tag{57}$$

which in effect represents the calibration curve. For nonspherical particles the analysis is kept general in terms of the particle mass.[107] Typical channel thicknesses are of the order of several hundred microns and spin rates are of the order of several hundred revolutions per minute,[107] although a recent design has used rates up to 32,000 r/min.[105]

An important feature of SFFF is that band broadening can easily be analyzed since the field is well defined. In consequence, one can use peak dispersion as a useful adjunct in combination with $R_F$ measurements.[107] The plate height, H, can be expressed under ideal conditions as[107]

$$H = \frac{\chi(\lambda')}{D} \langle v \rangle + \frac{9L_c\sigma_d^2}{D_p^2} \tag{58}$$

where $\sigma_d$ is the variance due to sample polydispersity; $L_c$ is the channel length; and $\langle v \rangle$ is the eluant average velocity. The parameter $\chi$ is a complex function of the reduced layer thickness, $\lambda'$. This equation predicts that a plot of H vs. mean velocity will yield a straight line, and from the slope, the diffusion coefficient, D. Combination of the slope with the Stokes-Einstein expression thus gives an independent cross-check on the particle diameter obtained from Equation 57. Extensive studies by Giddings et al. have confirmed these predictions for a series of monodisperse polystyrene latexes.[106,107] It is interesting to note that since hydrodynamic wall effects and electrostatic force field terms are not included in this analysis, their effect is presumably negligible, which contrasts sharply with the behavior of the packed column systems.

In a recent companion paper, an analysis of size distribution of a polydisperse PVC was carried out[108] using turbidimetric detection at 254 nm. Corrections for the scattering cross section and scale of the calibration curve were shown to be necessary for accurate determinations. Comparisons were made to transmission electron microscopy data and to disc centrifuge data. On a cumulative weight percentage basis, their results showed a consistent deviation of 22%, between microscopy and SFFF. By attributing the curve shift to the expected shrinkage of the latices under electron microscopy, the authors were able to show essential concordance.

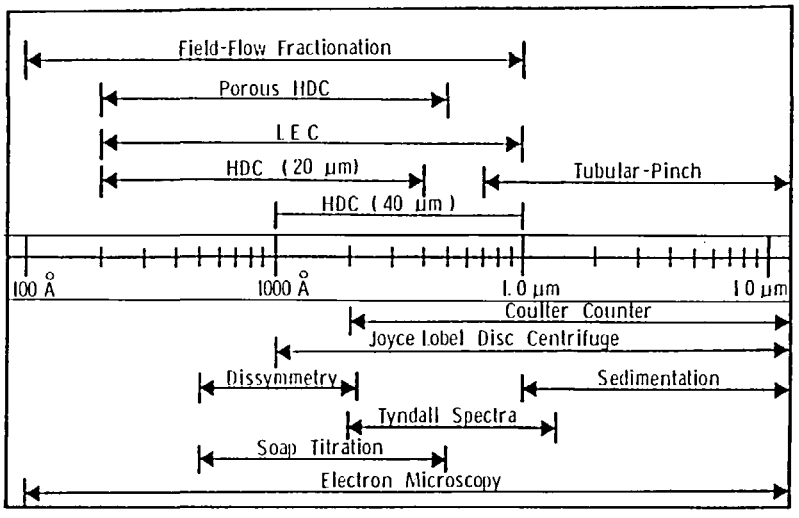


FIGURE 32. Applicable range of chromatographic and other common particle size analytical methods.



Studies over a wide range of eluant conditions with various latex systems are needed, however, at this point the method appears to have great promise as a relatively fast and easy-to-analyze technique for sizing colloidal particles. The added feature of spinning history programmability extends the range of its application while retaining its resolution.[109]

## VI. SUMMARY COMMENTS AND CONCLUSIONS

Figure 32 shows an illustration of the size ranges of the various methods of particle chromatography which have been discussed in this review. For comparison several of the other more commonly used methods are also shown. Under a given set of conditions, the size ranges of the chromatographic techniques can be extended somewhat, however, the illustration here is meant to point out the normal ranges of operation. In its present state of development, HDC is one of the most attractive methods in the submicron range. Since its speed, accuracy, and reproducibility have been independently verified by a number of workers, it seems to have stood the test of reliability. Its cost is relatively moderate, its operation is relatively straightforward, and as has been shown, its high performance potential for particle size distribution analysis has already been established. Further, a clear and fundamental understanding of the separation behavior has been developed which shows remarkable quantitative as well as qualitative behavior prediction. At the present time, a similar quantitative model for the dispersion behavior has not been developed, however, this has not substantially hampered the use of the technique for practical size distribution analysis. The methods of porous HDC show equal promise, however, studies leading to a clearer understanding of the separation mechanisms and/or more carefully designed packing materials are needed before the, perhaps ultimately greater, resolution potential of this method can be considered as well met as HDC.

For reasons discussed, it seems apparent that the open tubular methods will be restricted to particle analysis above 1 μm. However, in terms of ease of operation and range of particle and solvent conditions which can be handled, the method has much to offer as a practical, quality control tool.

Finally the methods of field-flow fractionation, only one of which has briefly been discussed here, offer a very substantial potential for advancement since by controlled "field

programming'' one has an additional resolution control. The method of sedimentation FFF appears to offer great promise as a result of its relative speed and theoretical directness. More complete studies of the resolving power for size distribution analysis are needed, but it may be that the ultimate choice between FFF and HDC will be based on cost and user preference.

Whatever the circumstances, it has hopefully been made clear by this review that the methods of particle chromatography have rapidly matured over the last 10 years to the status where they collectively can be considered as very important analytical tools for particle size analysis. Their applications to fundamental studies as well as their use as characterization tools should continue to grow at an increasing pace in the future.



## REFERENCES


1. **Cadle, R. D.,** *Particle Size,* Reinhold, New York, 1965.
2. **Allen, T.,** *Particle Size Measurement,* 2nd ed., Chapman & Hall, London, 1975.
3. **Collins, E. A., Davidson, J. A., and Daniels, C. A.,** Review of common methods of particle size measurement, *J. Paint Technol.*, 47, 35, 1975.
4. **Krebs, V. K. F. and Wunderlich, W.,** Die ermittlung der teilchengrobenverteilung von polymer-dispersionen durch gelchromatographie, *Angew. Makromol. Chem.*, 20, 203, 1971.
5. **Small, H.,** Hydrodynamic chromatography, a technique for size analysis of colloidal particles, *J. Colloid Interface Sci.*, 57, 337, 1976.
6. **Yau, W. W., Kirkland, J. J., and Bly, D. D.,** *Modern Size-Exclusion Liquid Chromatography,* John Wiley & Sons, New York, 1979.
7. **Flory, P. J.,** *Principles of Polymer Chemistry,* Cornell University Press, 1953, chap. 14.
8. **Friis, N. and Hamielec, A.,** Gel permeation chromatography: a review of axial dispersion phenomena, their detection, and correction, in *Advances in Chromatography,* Vol. 13, Giddings, J. C., Grushka, E., Keller, R. A., and Cazes, J., Eds., Marcel Dekker, New York, 1975, 41.
9. **McHugh, A. J., Nagy, D. J., and Silebi, C. A.,** Particle size analysis by chromatography, in *Size Exclusion Chromatography (GPC),* ACS Symp. Ser. 138, Provder, T., Ed., American Chemical Society, Washington, D.C., 1980, 1.
10. **Small, H., Saunders, F. L., and Solc, J.,** Hydrodynamic chromatography. A new approach to particle size analysis, *Adv. Colloid Interface Sci.*, 6, 237, 1976.
11. **Pedersen, K. O.,** Exclusion chromatography, *Arch. Biochem. Biophys.*, 1 (Suppl.), 157, 1962.
12. **DiMarzio, E. A. and Guttman, C. M.,** Separation by flow, *Macromolecules,* 3, 131, 1970.
13. **Guttman, C. M. and DiMarzio, E. A.,** Separation by flow. II. Application to gel permeation chromatography, *Macromolecules,* 3, 681, 1970.
14. **Verhoff, F. H. and Sylvester, N. D.,** Hydrodynamic fractionation of macromolecules. I. A simple theory, *J. Macromol. Sci.-Chem.*, A4(4), 979, 1970.
15. **Ruckenstein, E. and Prieve, D. C.,** Adsorption and desorption of particles and their chromatographic separation, *AIChE J.*, 22, 276, 1976.
16. **Ruckenstein, E., Marmur, A., and Gill, W. N.,** Feasibility of colloidal particles separation by potential barrier chromatography, *J. Colloid Interface Sci.*, 61, 183, 1977.
17. **Coll, H. and Fague, G. R.,** Liquid exclusion chromatography of colloidal dispersions, *J. Colloid Interface Sci.*, 76, 116, 1980.
18. **Singh, S. and Hamielec, A. E.,** Liquid exclusion chromatography. A technique for monitoring the growth of polymer particles in emulsion polymerization , *J. Appl. Polym. Sci.*, 22, 577, 1978.
19. **Mullins, M. E. and Orr, C.,** Particle sizing by capillary hydrodynamic chromatography, *Int. J. Multiphase Flow,* 5, 79, 1979.
20. **Noel, R. J., Gooding, K. M., Regnier, F. E., Ball, D. M., Orr, C., and Mullins, M. E.,** Capillary hydrodynamic chromatography, *J. Chromatogr.*, 166, 373, 1978.
21. **Giddings, J. C., Yang, F. J., and Myers, M. N.,** Theoretical and experimental characterization of flow field-flow fractionation, *Anal. Chem.*, 48, 1126, 1976.
22. **Giddings, J. C., Fisher, S. R., and Myers, M. N.,** Field-flow fractionation. One phase chromatography for macromolecules and particles, *Am. Lab.*, 10, 15, 1978.
23. **Giddings, J. C., Myers, M. N., and Moellmer, J. F.,** Fine-particle separation and characterization by field-flow fractionation, *J. Chromatogr.*, 149, 501, 1978.

24. **Stoisits, R. F., Poehlein, G. W., and Vanderhoff, J. W.,** Mathematical modelling of hydrodynamic chromatography, *J. Colloid Interface Sci.*, 57, 337, 1976.
25. **McHugh, A. J., Silebi, C., Poehlein, G. W., and Vanderhoff, J. W.,** Hydrodynamic chromatography of latex particles, *J. Colloid Interface Sci.*, 4, 549, 1976.
26. **Silebi, C. A. and McHugh, A. J.,** An analysis of flow separation in hydrodynamic chromatography of polymer latexes, *AIChE J.*, 24, 204, 1978.
27. **McGowan, G. R. and Langhorst, M. A.,** Development and application of an integrated, high-speed, computerized hydrodynamic chromatograph, *J. Colloid Interface Sci.*, 89, 94, 1982.
28. **Nagy, D. J., Silebi, C. A., and McHugh, A. J.,** Hydrodynamic chromatography — an evaluation of several features, *J. Colloid Interface Sci.*, 79, 264, 1981.
29. **Stoisits, R. F.,** Analysis of Colloids by Hydrodynamic Chromatography, M.S. thesis, Lehigh University, Bethlehem, 1975.
30. **Silebi, C. A. and McHugh, A. J.,** Particle size distribution of colloidal latexes by HDC, in *Emulsions, Latices, and Dispersions*, Becher, P. and Yudenfreund, M. N., Eds., Marcel Dekker, New York, 1978, 155.
31. **Meloan, C. E. and Kiser, R. W.,** *Problems and Experiments in Instrumental Analysis*, Merrill, Columbus, 1963, chap. 25.
32. **Nagy, D. J., Silebi, C. A., and McHugh, A. J.,** Latex particle size analysis by chromatographic methods: porous packed systems and detection of polystyrene, in *Polymer Colloids II*, Fitch, R. M., Ed., Plenum Press, New York, 1980, 121.
33. **Grubistic, Z., Rempp, R., and Benoit, H.,** A universal calibration for gel permeation chromatography, *J. Polym. Sci. Part B*, 5, 753, 1967.
34. **Nagy, D. J.,** Column Chromatography of Polymer Latexes, Ph.D. thesis, Lehigh University, Bethlehem, 1979.
35. **Brenner, H.,** Dynamics of neutrally buoyant particles in low Reynolds number flows, in *Progress in Heat and Mass Transfer*, Vol. 6, Hetsroni, G., Ed., Pergamon Press, New York, 1972, 509.
36. **Hiemenz, P. C.,** *Principles of Colloid and Surface Chemistry*, Marcel Dekker, New York, 1977.
37. **Prieve, D. C. and Hoysan, P. M.,** Role of colloidal forces in hydrodynamic chromatography, *J. Colloid Interface Sci.*, 64, 201, 1978.
38. **Buffham, B. A.,** Model-independent aspects of hydrodynamic chromatography theory, *J. Colloid Interface Sci.*, 67, 154, 1978.
39. **Brenner, H. and Gaydos, L. J.,** The constrained Brownian movement of spherical particles in cylindrical pores of comparable radius, *J. Colloid Interface Sci.*, 58, 312, 1977.
40. **Lee, H. L., Lightfoot, E. N., Reis, J. F. G., and Waissbluth, M. D.,** The systematic description and development of separation processes, in *Recent Developments in Separation Science*, Vol. 3, Part A, Li, N. N., Ed., CRC Press, Boca Raton, Fla., 1977, 1.
41. **Whitaker, S.,** Advances in theory of fluid motion in porous media, in *Flow Through Porous Media*, American Chemical Society, Washington, D.C., 1970, chap. 2.
42. **Novak, J., Janak, J., and Wicar, S.,** General description of the chromatographic process, in *Liquid Column Chromatography*, Vol. 3, Deyl, Z., Macek, K., and Janak, J., Eds., Elsevier, New York, 1975, chap. 3.
43. **Hermans, J.,** Role of diffusion in gel permeation chromatography, *J. Polym. Sci.*, 6 (A-2), 1217, 1968.
44. **Brenner, H.,** A general theory of Taylor dispersion phenomena, *Physicochem. Hydrodyn.*, 1, 91, 1980.
45. **Brenner, H.,** Dispersion resulting from flow through spatially periodic porous media, *Phil. Trans. R. Soc. Lond.*, A297, 81, 1980.
46. **Brenner, H. and Adler, P. M.,** Dispersion resulting from flow through spatially periodic porous media. II. Surface and intraparticle transport, *Phil. Trans. R. Soc. Lond.*, A307, 149, 1982.
47. **Bell, G. M., Levine, S., and McCartney, L. N.,** Approximate methods of determining the double-layer free energy of interaction between two charged colloidal spheres, *J. Colloid Interface Sci.*, 33, 335, 1970.
48. **Loeb, A. L., Wiersma, P. H., and Overbeek, J. Th. G.,** *The Electrical Double Layer Around a Spherical Particle*, MIT Press, Cambridge, 1961.
49. **Verwey, E. J. and Overbeek, J. Th. G.,** *Theory of the Stability of Lyophobic Colloids*, Elsevier, Amsterdam, 1948.
50. **Silebi, C. A.,** *Mathematical Modelling of Hydrodynamic Chromatography (HDC)*, Ph.D. thesis, Lehigh University, Bethlehem, 1977.
51. **Schaller, E. J. and Humphrey, A. E.,** Electroviscous effects in suspensions of monodisperse spherical particles, *J. Colloid Interface Sci.*, 22, 573, 1966.
52. **Clayfield, E. J. and Lumb, E. C.,** Detachment of adhered colloidal particles by non-aqueous surfactant solutions, *Disc. Faraday Soc.*, 42, 285, 1966.
53. **Gregory, J.,** Approximate expressions for retarded van der Waals interaction, *J. Colloid Interface Sci.*, 83, 138, 1981.

54. **Bird, R. B., Stewart, W. E., and Lightfoot, E. N.,** *Transport Phenomena*, John Wiley & Sons, New York, 1960.
55. **Visser, J.,** On Hamaker constants: a comparison between Hamaker constants and Lifshitz-van der Waals constants, *Adv. Colloid Interface Sci.*, 3, 331, 1972.
56. **Small, H.,** Hydrodynamic chromatography — a new approach to particle size analysis, presented at Cleveland-Akron GPC/LC Discussion Group Symposium on Liquid Chromatographic Methods, Cleveland, March 1977.
57. **Stigter, D. and Mysels, K. J.,** Tracer electrophoresis. II. The mobility of the micelle of sodium lauryl sulfate and its interpretation in terms of zeta potential and charge, *J. Phys. Chem.*, 59, 45, 1955.
58. **Coll, H., Fague, G. R., and Robillard, K. A.,** Exclusion chromatography of colloidal dispersions, unpublished manuscript, Eastman Kodak, Rochester, 1975.
59. **James, H. L., Gaylor, V. F., and Anthony, N. R.,** Liquid chromatographic techniques for measuring particle size in polymer latices, presented at Pittsburgh Conference on Analytical Chemistry, Cleveland, 1975.
60. **Johnston, J. E., Cowherd, C. L., and MacRury, T. B.,** Size exclusion chromatography of model latices: a feasibility study, in *Size Exclusion Chromatography (GPC)*, ACS Symp. Ser. 138, Provder, T., Ed., American Chemical Society, Washington, D.C., 1980, 27.
61. **Husain, A., Hamielec, A. E., and Vlachopoulos,** Particle size analysis using size exclusion chromatography, in *Size Exclusion Chromatography (GPC)*, ACS Symp. Ser. 138, Provder, T., Ed., American Chemical Society, Washington, D.C., 1980, 47.
62. **Nagy, D. J., Silebi, C. A., and McHugh, A. J.,** Resolution in column chromatography of polymer latexes. II. A comparison of porous and nonporous packing systems, *J. Appl. Polym. Sci.*, 26, 1567, 1981.
63. **Giddings, J. C., Kucera, E., Russell, C. P., and Myers, M. N.,** Statistical theory for the equilibrium distribution of rigid molecules in inert porous networks. Exclusion chromatography, *J. Phys. Chem.*, 72, 4397, 1968.
64. **Hamielec, A. E. and Singh, S.,** Chromatography of suspensions — an experimental and theoretical investigation of axial dispersion phenomena, *J. Liq. Chromatogr.*, 1(2), 187, 1978.
65. **Freeman, D. H. and Poienescu, I. C.,** Particle porosimetry by inverse gel permeation chromatography, *Anal. Chem.*, 49, 1183, 1978.
66. **Mori, S., Porter, R. S., and Johnson, J. F.,** Gel permeation chromatography: on the mechanism of separation by flow, *Anal. Chem.*, 46, 1599, 1974.
67. **Francis, D. C.,** A Mathematical Model of Porous Hydrodynamic Chromatography, M.S. thesis, University of Illinois, Urbana, 1983.
68. **McHugh, A. J. and Francis, D. C.,** Mechanisms of particle chromatography, *Org. Coat. Appl. Polym. Sci.*, 48, 599, 1983, full paper submitted for publication in *Recent Advances in Size Exclusion Chromatography*, Provder, T., Ed., American Chemical Society, Washington, D.C., in press.
69. **Casassa, E. F.,** Theoretical models for peak migration in gel permeation chromatography, *J. Phys. Chem.*, 75, 3929, 1971.
70. **Horn, F. J. M.,** Calculation of dispersion coefficients by means of moments, *AIChE J.*, 17, 613, 1971.
71. **Reis, J. R. G., Lightfoot, E. N., Noble, P. T., and Chiang, A. S.,** Chromatography in a bed of spheres, *Sep. Sci. Tech.*, 14(5), 367, 1979.
72. **Ouano, A. C. and Barker, J. A.,** A computer simulation of linear gel permeation chromatography, *Sep. Sci.*, 8(6), 673, 1973.
73. **Yau, W. W. and Malone, C. P.,** An approach to diffusion theory of gel permeation chromatographic separation, *Polym. Lett.*, 5, 663, 1967.
74. **Chang, T. L.,** On the separation mechanism of gel permeation chromatography, *Anal. Chim. Acta*, 42, 51, 1968.
75. **Yau, W. W.,** Steric exclusion and lateral diffusion in gel-permeation chromatography, *J. Polym. Sci.*, 7 (PtA-2), 483, 1969.
76. **Yau, W. W., Malone, C. P., and Suchan, H. L.,** Separation mechanisms in gel permeation chromatography, *Sep. Sci.*, 5(3), 259, 1970.
77. **Athey, R. D., Provder, T., Poehlein, G. W., and Scolere, J.,** Hydrodynamic volume evidence for swellability of stryene-butadiene carboxylated latexes, *Coll. Polym. Sci.*, 255, 1001, 1977.
78. **Tung, L. H.,** Method of calculating molecular weight distribution function from gel permeation chromatograms, *J. Appl. Polym. Sci.*, 10, 37, 1966; Correction of instrument spreading in gel permation chromatography, *J. Appl. Polym. Sci.*, 13, 775, 1969.
79. **Silebi, C. A. and McHugh, A. J.,** The determination of particle size distributions by hydrodynamic chromatography. An analysis of dispersion and methods for improved signal resolution, *J. Appl. Polym. Sci.*, 23, 1699, 1979.
80. **Husain, A., Vlachopoulos, J., and Hamielec, A. E.,** Chromatography of suspensions — analytical corrections for axial dispersion, *J. Liq. Chromatogr.*, 2(2), 193, 1979.

81. **Husain, A., Vlachopoulos, J., and Hamielec, A. E.,** Chromatography of suspensions. An absolute particle size detector based on turbidity-spectra analysis — a similation study, *J. Liq. Chromatogr.*, 2(4), 517, 1979.
82. **Provder, T. and Rosen, E. M.,** The instrument spreading correction in GPC. I. The general shape function using a linear calibration curve, *Sep. Sci.*, 5(4), 437, 1970.
83. **Husain, A., Hamielec, A. E., and Vlachopoulos, J.,** An analysis of imperfect resolution in the chromatography of particle suspensions, *J. Liq. Chromatogr.*, 4(3), 425, 1981.
84. **Husain, A., Hamielec, A. E., and Vlachopoulos, J.,** A new method for identifying and estimating the parameters of the instrumental spreading function in size exclusion chromatography — an application to particle size analysis, *J. Liq. Chromatogr.*, 4(3), 459, 1981.
85. **Van de Hulst, A. C.,** *Light Scattering by Small Particles*, Dover, New York, 1981, 14.
86. **Silebi, C. A. and Viola, J. P.,** A theoretical and experimental examination of axial dispersion in hydrodynamic chromatography (HDC), *Org. Coat. Plast. Chem.*, 42, 151, 1980.
87. **Kelley, R. N. and Billmeyer, F. W.,** Evaluating dispersion in gel permeation chromatography, *Anal. Chem.*, 41, 874, 1969.
88. **Haller, W.,** Chromatography on glass of controlled pore size, *Nature (London)*, 206, 693, 1965.
89. **Kirkland, J. J.,** High-performance size-exclusion liquid chromatography of inorganic colloids, *J. Liq. Chromatogr.*, 185, 273, 1979.
90. **Dubin, P. L.,** Size exclusion chromatography of some reversed micellar systems, in *Size Exclusion Chromatography (HDC)*, ACS Symp. Ser. 138, Provder, T., Ed., American Chemical Society, Washington, D.C., 1980, 225.
91. **Prud'homme, R. K., Froiman, G., and Hoagland, D. A.,** Molecular size determination of xanthan polysaccharide, *Carbohydr. Res.*, 106, 225, 1982.
92. **Prud'homme, R. K. and Hoagland, D. A.,** Orientation of rigid macromolecules during hydrodynamic chromatography separations, *Sep. Sci.*, in press.
93. **Hoagland, D. A., Larson, K. A., and Prud'homme, R. K.,** HDC separations of high molecular weight water soluble polymers, in *Modern Methods of Particle Size Analysis*, ACS Symp. Ser. Bartle, H., Ed., American Chemical Society, Washington, D.C., in press.
94. **Lecourtier, J. and Chauveteau, G.,** Xanthan fractionation by surface exclusion chromatography, *Macromolecules*, submitted.
95. **Shawki, S. M. and Hamielec, A. E.,** The effect of shear rate on molecular weight determination of acrylamide polymers from intrinsic viscosity measurements, *J. Appl. Polym. Sci.*, 23, 3323, 1979.
96. **Barth, M. G. and Regnier, F. E.,** High performance gel permeation chromatography of water-soluble cellulosics, *J. Chromatogr.*, 192, 275, 1980.
97. **Segré, G. and Silberberg, A.,** Behavior of macroscopic rigid spheres in Pouiseuille flow. II. Experimental results and interpretation, *J. Fluid Mech.*, 14, 136, 1962.
98. **Tremblay, R. D., Penrose, J. T., and Trumbore, C. N.,** Evidence for molecular separations in stainless steel capillary HPLC tubing, paper presented at ACS Meeting, Washington, D.C., September 1979.
99. **Poehlein, S.,** Capillary chromatography, unpublished research report, Lehigh University, Bethlehem, 1978.
100. **Karnis, A., Goldsmith, H. L., and Mason, S. G.,** The flow of suspensions through tubes. V. Inertial effects, *Can. J. Chem. Eng.*, 44, 181, 1966.
101. **Walz, D. and Grum, F.,** The radial velocity of spherical particles in tubular pinch effect experiments, *J. Colloid Interface Sci.*, 45, 467, 1973.
102. **Giddings, J. C.,** Basic approaches to separation. Analysis and classification of methods according to underlying transport characteristics, *Sep. Sci. Technol.*, 13(1), 3, 1978.
103. **Giddings, J. C.,** Displacement and dispersion of particles of finite size in flow channels with lateral forces. Field-flow fractionation and hydrodynamic chromatography, *Sep. Sci. Technol.*, 13(3), 241, 1978.
104. **Giddings, J. C., Myers, M. N., Caldwell, K. D., and Fisher, S. R.,** Analysis of biological macromolecules and particles by field-flow fractionation, in *Methods of Biochemical Analysis*, Vol. 26, Glick, D., Ed., John Wiley & Sons, New York, 1980, 79.
105. **Kirkland, J. J., Dilks, C. H., and Yau, W. W.,** Sedimentation field flow fractionation at high force field, *J. Chromatogr.*, 255, 255, 1983.
106. **Giddings, J. C., Yang, F. J. F., and Myers, M. N.,** Sedimentation field-flow fractionation, *Anal. Chem.*, 46, 1917, 1974.
107. **Giddings, J. C., Karaiskakis, G., Caldwell, K. D., and Myers, M. N.,** Colloid characterization by sedimentation field-flow fractionation. I. Monodisperse populations, *J. Colloid Interface Sci.*, 92, 66, 1983.
108. **Yang, F. S., Caldwell, K. D., and Giddings, J. C.,** Colloid characterization by sedimentation field-flow fractionation. II. Particle size distribution, *J. Colloid Interface Sci.*, 92, 81, 1983.
109. **Yang, F. J. F., Myers, M. N., and Giddings, J. C.,** Programmed sedimentation field-flow fractionation, *Anal. Chem.*, 46, 1924, 1974.
110. **Brough, A. W. J., Hillman, D. E., and Perry, R. W.,** Capillary hydrodynamic chromatography — an investigation into operational characteristics, *J. Chromatogr.*, 208, 175, 1981.

111. **Oshima, H., Healy, T. W., and White, L. R.,** Accurate analytic expressions for the surface charge density/surface potential relationship and double-layer potential distribution for a spherical colloidal particle, *J. Colloid Interface Sci.*, 90, 11, 1982.
112. **Saffman, P. G.,** Dispersion due to molecular diffusion and macroscopic mixing in flow through a network of capillaries, *J. Fluid Mech.*, 7, 194, 1960.
113. **Nagy, D. J., Silebi, C. A., and McHugh, A. J.,** Resolution in column chromatography of polymer latexes. I. The light scattering behavior of polystyrene and its effect on signal resolution in HDC, *J. Appl. Polym. Sci.*, 26, 1555, 1981.
114. **Brenner, H.,** Hydrodynamic resistance of particles at small Reynolds numbers, *Adv. Chem. Eng.*, 6, 287, 1966.
115. **Leal, L. G.,** Particle motions in a viscous fluid, *Ann. Rev. Fluid Mech.*, 12, 435, 1980.
116. **Nagy, D. J.,** Hydrodynamic chromatography: a further evaluation of universal calibration, *J. Colloid Interface Sci.*, 93, 590, 1983.